Gallium neutrino absorption cross section and its uncertainty

S. R. Elliott [1], V. N. Gavrin,[2] W. C. Haxton [3,4,*] T. V. Ibragimova,[2] and E. J. Rule [3]

[1]*Los Alamos National Laboratory, Los Alamos, New Mexico 87545, USA*
[2]*Institute for Nuclear Research of the Russian Academy of Sciences, Moscow 117312, Russia*
[3]*Department of Physics, University of California, Berkeley, California 94720, USA*
[4]*Lawrence Berkeley National Laboratory, Berkeley, California 94720, USA*

In the recent Baksan Experiment on Sterile Transitions (BEST), a suppressed rate of neutrino absorption on a gallium target was observed, consistent with earlier results from neutrino source calibrations of the SAGE and GALLEX/GNO solar neutrino experiments. The BEST Collaboration, utilizing a 3.4 MCi ^{51}Cr neutrino source, found observed-to-expected counting rates at two very short baselines of $R = 0.791 \pm 0.05$ and 0.766 ± 0.05, respectively. Among recent neutrino experiments, BEST is notable for the simplicity of both its neutrino spectrum, line neutrinos from an electron-capture source whose intensity can be measured to a estimated precision of 0.23%, and its absorption cross section, where the precisely known rate of electron capture to the gallium ground state, ^{71}Ge$(e^-, \nu_e)^{71}$Ga(g.s.), establishes a minimum value. However, the absorption cross section uncertainty is a common systematic in the BEST, SAGE, and GALLEX/GNO neutrino source experiments. Here we update that cross section, considering a variety of electroweak corrections and the role of transitions to excited states, to establish both a central value and reasonable uncertainty, thereby enabling a more accurate assessment of the statistical significance of the gallium anomalies. Results are given for ^{51}Cr and ^{37}Ar sources. The revised neutrino capture rates are used in a reevaluation of the BEST and gallium anomalies.

I. INTRODUCTION: THE Ga NEUTRINO ANOMALY

The possibility of additional, very weakly interacting "sterile" neutrinos, beyond the three light neutrinos of the standard model, has been raised frequently in the literature [1–8]. They arise naturally in extensions of the standard model that account for nonzero neutrino masses. Sterile neutrinos have been discussed in connection with the LSND experiment, the reactor neutrino anomaly, the SAGE and GALLEX/GNO neutrino calibration experiments, and with efforts to reconcile oscillation parameters derived from experiments T2K and NOvA [1,7,9].

In the radiochemical SAGE and GALLEX/GNO solar neutrino experiments, a large mass of Ga (30–50 tons) was exposed to the solar neutrino flux for a period of about a month, during which neutrino capture occurs via ^{71}Ga$(\nu_e, e^-)^{71}$Ge. The produced atoms of radioactive ^{71}Ge, $\tau_{1/2} = 11.43 \pm 0.03$ d, were then chemically extracted and counted as they decay back to ^{71}Ga via electron capture. These experiments established capture rates that, in combination with those from the chlorine and Kamioka experiments, indicated a pattern of solar neutrino fluxes that could not be easily reconciled with solar models, helping to motivate a new generation of solar neutrino detectors: Super-Kamiokande [10], the Sudbury Neutrino Observatory [11], and Borexino [12,13]. This led to the discovery of neutrino mass and oscillations and the detection of an energy-dependent distortion of the solar

neutrino flux, reflecting the interplay between vacuum and matter-enhanced oscillations [14,15].

While both gallium experiments utilized tracers to demonstrate the reliability of the chemical extraction, direct cross checks on their overall efficiencies for neutrino detection were also performed. Intense ^{51}Cr and ^{37}Ar electron-capture (EC) neutrino sources of known strength were placed at the center of the Ga targets, and the additional production of ^{71}Ge was measured. Four such calibrations [16–19] were performed, which when combined yield a ratio of the observed to expected counting rates of $R = 0.866 \pm 0.054$. The discrepancy between this result and $R = 1$ is known as the gallium anomaly.

The gallium anomaly and other short-baseline neutrino discrepancies motivated the recent Baksan Experiment on Sterile Transitions (BEST) [20,21]. BEST, employing an exceptionally intense 3.4 MCi ^{51}Cr neutrino source, measured the rate of neutrino reactions at two distances by dividing the Ga target reactor into inner and outer volumes. This opened up the possibility of detecting an oscillation signal. While no distance dependence was seen, the counting rates were again well below expectations, with $R = 0.791 \pm 0.05$ and 0.766 ± 0.05 for the inner (shorter baseline) and outer volumes, respectively.

A critical issue in the analysis of BEST and earlier Ga neutrino source experiments is the cross section for ^{71}Ga$(\nu_e, e^-)^{71}$Ge, as this is a common systematic in these measurements. For ^{51}Cr and ^{37}Ar neutrino sources, the contributing transitions from the ^{71}Ga ground state are to the ground state and first two excited states of ^{71}Ge, as shown

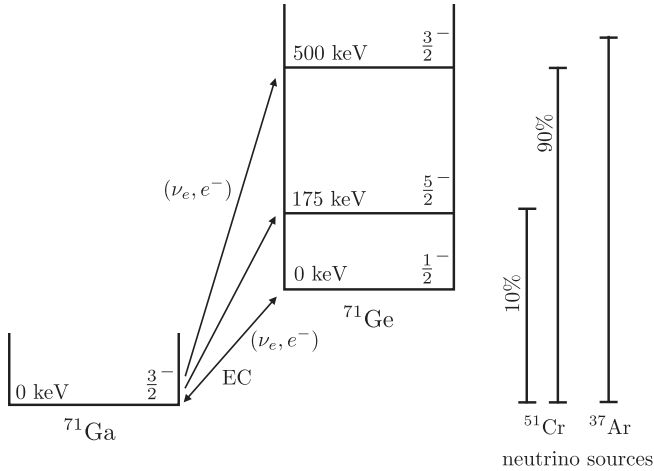*Corresponding author: haxton@berkeley.edu

FIG. 1. Level diagram for $^{71}\text{Ga}(\nu_e, e^-)^{71}\text{Ga}$ showing the states that contribute to the absorption of ^{51}Cr and ^{37}Ar EC neutrinos.

in Fig. 1. The Ga anomaly cannot be attributed entirely to uncertainties in the neutrino cross section, due to the dominance of the strong $\frac{3}{2}^- \rightarrow \frac{1}{2}^-$ transition to the ^{71}Ge ground state, as this transition strength is precisely determined by the known EC rate of ^{71}Ge. Even if only this contribution is included, a $\approx 2\sigma$ discrepancy remains. In addition, two allowed Gamow-Teller (GT) transitions to ^{71}Ge excited states, the $\frac{5}{2}^-$ and $\frac{3}{2}^-$ levels at 175 and 500 keV, respectively, also contribute to the total ^{51}Cr neutrino absorption cross section. The contributions of these transitions have generally been deduced from surrogate probes of GT strength—forward-angle (p, n) or $(^3\text{He}, t)$ scattering—despite long-established concerns about the reliability of these probes when applied to specific weak transitions [22,23].

While one cannot attribute the Ga anomaly entirely to nuclear physics, the central value and uncertainty of the cross section can influence the statistical significance of the BEST

result, its possible interpretation in terms of new physics, and its consistency with other tests of neutrino properties. The purpose of this paper is to (1) reexamine the relationship between the $^{71}\text{Ge}(\text{g.s.})(e^-, \nu_e)^{71}\text{Ga}(\text{g.s.})$ electron capture rate and the $^{71}\text{Ga}(\text{g.s.})(\nu_e, e^-)^{71}\text{Ge}(\text{g.s.})$ cross section, in order to deduce the best value and uncertainty of the latter; and (2) reconsider the excited-state contributions in light of new data testing the proportionality between (p, n) or $(^3\text{He}, t)$ cross sections and experimentally known weak rates. In (1), we examine (or reexamine) several $\approx 1\%$ corrections that can impact the proportionality between the g.s. $\leftrightarrow$ g.s. inverse reactions. In (2), our focus is on defining a reasonable uncertainty for the excited state contribution, based on a critical examination of the reliability of such surrogate interactions as probes of specific weak GT transitions.

II. THE ^{71}Ge ELECTRON CAPTURE RATE

One would like to derive from the known electron capture rate for ^{71}Ge the strength of the ground-state GT transition of the inverse neutrino reaction cross section. In addition to the half-life [24,25],

$$\tau_{\frac{1}{2}}[^{71}\text{Ge}] = 11.43 \pm 0.03 \text{ d}, \quad (1)$$

relevant experimental information includes the Q_{EC} value for the decay [26], the difference in the atomic masses

$$\begin{aligned} Q_{\text{EC}} &= M[^{71}\text{Ge}] - M[^{71}\text{Ga}] \\ &= 232.443 \pm 0.093 \text{ keV}, \end{aligned} \quad (2)$$

and the P_K, P_L, and P_M electron-capture probabilities and associated atomic binding energies [27],

$$\begin{aligned} P_K &= 0.88, & E_{\text{bind}} &= 10.37 \text{ keV}, \\ P_L &= 0.103, & E_{\text{bind}} &= 1.2 \text{ keV}, \\ P_M &= 0.017, & E_{\text{bind}} &= 0.12 \text{ keV}. \end{aligned} \quad (3)$$

The $^{71}\text{Ge} \rightarrow {}^{71}\text{Ga}$ electron capture rate can then be written

$$\omega = \frac{\ln[2]}{\tau_{\frac{1}{2}}} = \frac{G_F^2 \cos^2\theta_C}{2\pi} |\phi_{1s}|^2_{\text{avg}} E_{\nu,1s}^2 \left[2\left(1 + \epsilon_o^{1s}\right)\left(1 + \frac{P_L + P_M}{P_K}\right) \right] g_A^2 \left[2\,\text{B}_{\text{GT}}^{(\nu,e)}(\text{g.s.}) \right] [1 + g_{\nu,b}]_{\text{EC}} [1 + \epsilon_q]. \quad (4)$$

The various terms appearing above are as follows:

(1) *Q value.* The neutrino energy $E_{\nu,1s}$ for electron K capture. Neglecting a very small nuclear recoil correction, it is given by the energy constraint

$$Q_{\text{EC}} = E_{\nu,1s} + 10.37\text{keV}$$
$$\Rightarrow E_{\nu,1s} = 222.1 \pm 0.1\text{keV}$$

(2) *Branchings.* The factor $[2(1 + \epsilon_o^{1s})(1 + \frac{P_L + P_M}{P_K})]$ relates the total capture rate to the rate for capture of a single $1s$ electron, with the contributions of L and M capture included through use of the experimentally

known branching ratios. This procedure requires the introduction of a rearrangement (or overlap-exchange) correction ϵ_0^{1s} to account for the imperfect overlap of the state created by annihilating a $1s$ electron in the ^{71}Ge atomic ground state, with states appropriate for the Coulomb field of ^{71}Ga. That is, while the instantaneous annihilation of the $1s$ electron in ^{71}Ge will lead dominantly to a virtual state that decays by emitting K-capture Auger electrons and x rays, atomic rearrangement generates small contributions from L and M capture. Similar corrections would be needed for other channels. That is, the total rate would be

proportional to

$$\sum_i |\phi_i|^2_{\text{avg}} E^2_{\nu,i}\left(1+\epsilon^i_o\right) = |\phi_{1s}|^2_{\text{avg}} E^2_{\nu,1s}\left(1+\epsilon^{1s}_o\right)\left[1+\frac{\sum_{i\neq 1s}|\phi_i|^2_{\text{avg}} E^2_{\nu,i}\left(1+\epsilon^i_o\right)}{|\phi_{1s}|^2_{\text{avg}} E^2_{\nu,1s}\left(1+\epsilon^{1s}_o\right)}\right] = |\phi_{1s}|^2_{\text{avg}} E^2_{\nu,1s}\left(1+\epsilon^{1s}_o\right)\left[1+\frac{P_L+P_M}{P_K}\right] \quad (5)$$

where $|\phi_i|^2_{\text{avg}}$ is the K, L, or M atomic density at the nucleus, $E_{\nu,i}$ is the associated energy of the emitted neutrino, and ϵ^i_o is the overlap and exchange correction needed in the ith channel [28–31]. Bahcall [30] noted that such corrections to theory were needed to reproduce precise experimental L/K capture ratios and estimated their sizes. As he has emphasized, if the theoretical expression on the left-hand side of Eq. (5) is used, the inclusion of the ϵ_i would have little net impact, as these factors diminish P_K but enhance P_L and P_M. Here, however, we make use of the experimentally measured probabilities P_K, P_L, and P_M to write the total rate in terms of the $1s$-capture rate, so inclusion of overlap/exchange correction for the $1s$ channel is needed.

The values for ϵ^{1s}_o given by Bahcall [30,32–34] and by Vatai [31] are -0.018 and -0.008, respectively. Though the correction is small, there is a relatively large fractional difference between the results. [In contrast, their corrections for L (0.083 and 0.088, respectively) and M (0.247 and 0.188, respectively) capture are in better agreement, with fractional differences of 6% and 31%, respectively]. We adopt as a nominal value the average and take twice the standard deviation as the 95% confidence level (C.L.), yielding $\epsilon^{1s}_o = -0.013 \pm 0.014$ and

$$\left(1+\epsilon^{1s}_o\right)\left(1+\frac{P_L+P_M}{P_K}\right) = 1.122 \pm 0.016.$$

(3) *Weak couplings.* We adopt Particle Data Group (PDG) values for the Fermi constant, $G_F/(\hbar c)^3 = 1.1664 \times 10^{-5}/\text{GeV}^2$, and Cabibbo angle, $\cos\theta_C = 0.9743$, and the PERKEO III value [35] for the axial vector coupling $g_A = 1.2764$. (The PERKEO III experiment employed a novel pulsed cold neutron source to greatly reduce systematic uncertainties, yielding a result that is both exceptionally precise and statistics dominated. The PDG value for g_A employs an error-bar inflation of 2.7 to account for the scatter among past experiments, thereby eroding the impact of the new technique.)

Note, however, that the choice of weak couplings and their uncertainties do not influence our results. As all transition rates are taken from experiment, any change in the weak couplings would be absorbed into the fitted BGT value. Weak coupling uncertainties—whether taken from the PDG or elsewhere—are too small to influence the overall error budget of our cross section calculations.

(4) *Electron density at the nucleus.* $|\phi_{1s}|^2_{\text{avg}}$ is the ^{71}Ge $1s$ atomic density at the nucleus. The nuclear amplitudes for the EC transitions of interest involve convolutions of the GT operator—the space-like component of the

nuclear axial current—with leptonic wave functions,

$$\langle j_f|\int d\boldsymbol{r}\,\phi^*_{\nu_e}(\boldsymbol{r})\phi_{1s}(\boldsymbol{r})\sum_{i=1}^A \boldsymbol{\sigma}(i)\tau_-(i)\delta(\boldsymbol{r}-\boldsymbol{r}_i)|j_i\rangle$$

where we abbreviate the nuclear ground states of ^{71}Ge and ^{71}Ga as $|j_i\rangle$ and $|j_f\rangle$, respectively. As $q_\nu R_N \ll 1$, where R_N is the nuclear radius and q_ν is the magnitude of the neutrino's three-momentum, one can approximate the neutrino plane wave within the nucleus by $\phi^*_{\nu_e}(\boldsymbol{r}) \approx 1$. (The leading correction to this approximation will be evaluated below.) Similarly, given that the atomic wave function varies slowly over the nuclear scale, $\phi_{1s}(\boldsymbol{r})$ can be removed from the integral and replaced by an average value. Most commonly $|\phi_{1s}|_{\text{avg}}$ is computed by folding the electron probability density with the normalized ^{71}Ge proton charge distribution, then integrating over the nuclear volume.

In his 1997 work [36], Bahcall used three relativistic, self-consistent Hartree-Fock calculations that took into account the finite extent of the nucleus, the Breit interaction, vacuum polarization, and self-energy corrections, averaging the resulting wave functions over the nuclear volume to obtain $|\phi_i|^2_{\text{avg}}$ for K, L, and M capture. The calculations, performed by three independent groups, agreed at the $\pm 0.2\%$ level. We are not aware of any subsequent calculations that are as complete. While [36] includes references to the atomic methods employed by the three groups, the ^{71}Ge results were provided as private communications and are not described in separate publications. As the relationship between the dimensionless numerical quantity given in [36] and the density $|\phi_{1s}|_{\text{avg}}$ may not be obvious to readers, we provide some of the needed definitions here.

The dimensionless quantity evaluated in [36], given by the quantity in square brackets below, is related to the dimensionful quantities we define on the left below by

$$\sum_i |\phi_i|^2_{\text{avg}} E^2_{\nu,i} = \frac{(m_e c^2)^5}{(\hbar c)^3}\frac{1}{4\pi}\left[\sum_i g_i^2 \tilde{E}^2_{\nu,i}\right] \quad (6)$$

where $\tilde{E}_{\nu,i} \equiv E_{\nu,i}/m_e c^2$. The factor of $1/4\pi$ appears because Bahcall evaluated the s-wave radial density, not the full density. As the square-bracketed quantity depends on Q_{EC}, a small correction is needed because $Q_{\text{EC}} = 232.69$ keV was used in [36], while the current value is given by Eq. (2). Plugging in the numerical

values from [36] one finds

$$
\left[\sum_i g_i^2 \tilde{E}_{v,i}^2\right]^{Q_{EC}=232.443\text{keV}}
$$

$$
\approx 0.9978 \left[\sum_i g_i^2 \tilde{E}_{v,i}^2\right]^{Q_{EC}=232.69\text{keV}}
$$

$$
= 0.01440 \tag{7}
$$

We again group terms so that we can use experimental EC ratios, finding from Eqs. (6) and (7)

$$
\frac{(m_e c^2)^5}{(\hbar c)^3} \frac{0.01440}{4\pi}
$$

$$
= |\phi_{1s}|_{\text{avg}}^2 E_{v,1s}^2 \left[1 + \frac{1+\epsilon_o^{1s}}{1+\epsilon_o^L}\frac{P_L}{P_K} + \frac{1+\epsilon_o^{1s}}{1+\epsilon_o^M}\frac{P_M}{P_K}\right]
$$

$$
= |\phi_{1s}|_{\text{avg}}^2 E_{v,1s}^2 \begin{cases} 1.121, & \text{Bahcall}, \\ 1.123, & \text{Vatai}, \end{cases} \tag{8}
$$

where the overlap and exchange factors arise because, following Eq. (5), canceling terms are implicitly included in the probabilities P_K, P_L, and P_M. We find the result depends only weakly on whether we take these corrections from [30] or from [31]. Evaluating this expression yields

$$
(\hbar c)^3 |\phi_{1s}|_{\text{avg}}^2 = (7.21 \pm 0.03) \times 10^{-4} \text{ MeV}^3 \tag{9}
$$

The uncertainty is determined from the standard deviations of the three atomic calculations reported in [36] and of the overlap and the exchange corrections of Bahcall and Vatai. These are combined in quadrature, then doubled to give the 95% C.L. range given in Eq. (9). This procedure thus takes into account differences apparent from the spread among competing calculations, but not those that could arise if the calculations being compared employed common but flawed assumptions.

One can recast this numerical result in terms of a more familiar density, the Schrödinger density for an electron bound to a point charge Z, evaluated at the origin. One finds

$$
(\hbar c)^3 |\phi_{1s}|_{\text{avg}}^2 = R\frac{(Z\alpha m_e c^2)^3}{\pi}\bigg|_{Z=32}, \tag{10}
$$

where Eq. (9) determines the numerical proportionality factor, $R = 1.333$.

(5) B_{GT} *convention.* In this paper, all B_{GT} values are given for the neutrino reaction direction, $^{71}\text{Ga}(\nu_e, e^-)^{71}\text{Ge}$. For the g.s. $\rightarrow$ g.s. EC direction,

$$
B_{\text{GT}}^{\text{EC}}(\text{g.s.})
$$

$$
= \frac{1}{2j_i+1}\left|\left\langle j_f = \frac{3}{2}\left|\left|\sum_{1}^{A}\boldsymbol{\sigma}(i)\tau_-(i)\right|\right|j_i = \frac{1}{2}\right\rangle\right|^2
$$

$$
= \frac{2}{2j_i+1}\left|\left\langle j_f = \frac{1}{2}\left|\left|\sum_{1}^{A}\boldsymbol{\sigma}(i)\tau_+(i)\right|\right|j_i = \frac{3}{2}\right\rangle\right|^2
$$

$$
\equiv 2 B_{\text{GT}}^{(\nu,e)}(\text{g.s.}). \tag{11}
$$

Thus, $B_{\text{GT}}^{\text{EC}}(\text{g.s.})$ is given as $2B_{\text{GT}}^{(\nu,e)}(\text{g.s.})$ in Eq. (4).

(6) *Weak magnetism correction.* $[1 + \epsilon_q]$ is the correction to B_{GT} arising from contributions beyond the allowed approximation. Because of the very low momentum transfer, these corrections are expected to be small and dominated by the interference term between the GT amplitude and weak magnetism. This interference generates a term linear in the three-momentum transfer. We find a correction to the GT transition probability of

$$
\epsilon_q = \frac{2E_{v,1s}}{3m_N g_A}\left[\mu_{T=1} + \frac{\left\langle\frac{3}{2}^-\left|\left|\sum_{i=1}^{A}\boldsymbol{\ell}(i)\tau_-(i)\right|\right|\frac{1}{2}^-\right\rangle}{\left\langle\frac{3}{2}^-\left|\left|\sum_{i=1}^{A}\boldsymbol{\sigma}(i)\tau_-(i)\right|\right|\frac{1}{2}^-\right\rangle}\right], \tag{12}
$$

where m_N is the nucleon mass and $\mu_{T=1} \approx 4.706$ is the isovector magnetic moment. As the spin contribution to weak magnetism is effectively determined by the EC capture rate, only the orbital contribution must be taken from theory.

While the large isovector magnetic moment makes the weak magnetism correction relatively insensitive to nuclear structure uncertainties, one still must estimate the orbital contribution. We do this using the shell model (SM), retaining all Slater determinants within the $2p_{3/2}1f_{5/2}2p_{1/2}1g_{9/2}$ model space, and employing three effective interactions designed for this space, GCN2850 [37], jj44b [38], and JUN45 [39].

We selected these interactions because of the extensive literature comparing their predictions to experiment, specifically, how well they reproduce measured moments, transitions, and low-lying nuclear spectra. For example, in [39] comparisons are made to experiment for binding energies, magnetic and quadrupole moments, $B(E2)$ values, and nuclear spectra of a large set of $2p_{3/2}1f_{5/2}2p_{1/2}1g_{9/2}$ nuclei, including both ^{71}Ga and ^{71}Ge. In the paper presenting the jj44b interaction [38], the properties and spectroscopy of odd isotopes of Ga (including ^{71}Ga) were used as test of its quality. Side-by-side comparisons of JUN45 and jj44b predictions for spectra, quadrupole moments, and $B(E2)$ values for the even isotopes of Ge are made in [40,41], and for the odd-isotopes of Ga (including ^{71}Ga) in [42]. The literature on GCN2850 predictions is somewhat more limited: the interaction has been employed in studies of weak processes such as $\beta\beta$ decay (^{76}Ge) and WIMP scattering (^{73}Ge). Representative work includes [43–45].

The dimension of the SM space for ^{71}Ge is about 1.5×10^8. The diagonalizations were performed with the Lanczos-algorithm code BIGSTICK [46,47]. We found

$$
\left\langle\frac{3}{2}^-\left|\left|\sum_{i=1}^{A}\boldsymbol{\ell}(i)\tau_-(i)\right|\right|\frac{1}{2}^-\right\rangle = \begin{cases} 0.48, & \text{GCN2850}, \\ 0.69, & \text{jj44b}, \\ 0.005, & \text{JUN45}, \end{cases}
$$

so that the ratio that enters in Eq. (12) is

$$\frac{\left\langle \frac{3}{2}^- \left\| \sum_{i=1}^A \boldsymbol{\ell}(i)\tau_-(i) \right\| \frac{1}{2}^- \right\rangle}{\left\langle \frac{3}{2}^- \left\| \sum_{i=1}^A \boldsymbol{\sigma}(i)\tau_-(i) \right\| \frac{1}{2}^- \right\rangle_{\text{exp}}}$$

$$= \begin{cases} -0.81, & \text{GCN2850,} \\ -1.18, & \text{jj44b,} \\ -0.01, & \text{JUN45,} \end{cases}$$

where the magnitude of the GT matrix element is taken from experiment, while the relative sign is the SM prediction. From the average and standard deviation of these theory results, we find

$$\frac{\left\langle \frac{3}{2}^- \left\| \sum_{i=1}^A \boldsymbol{\ell}(i)\tau_-(i) \right\| \frac{1}{2}^- \right\rangle}{\left\langle \frac{3}{2}^- \left\| \sum_{i=1}^A \boldsymbol{\sigma}(i)\tau_-(i) \right\| \frac{1}{2}^- \right\rangle_{\text{exp}}}$$

$$= -0.7 \pm 1.2 \quad (95\% \text{ C.L.})$$

where the assigned uncertainty is again twice the standard deviation. Because the large isovector magnetic moment dominates Eq. (12), the estimate of the forbidden corrections is relatively stable, despite substantial differences in the SM estimates of the orbital angular momentum matrix element. The end result

$$\epsilon_q = (4.9 \pm 1.5) \times 10^{-4} \quad (95\% \text{ C.L.})$$

shows that the weak magnetism correction is negligible. We have also evaluated this correction using the full momentum dependence of the weak transition amplitude, doing a standard multipole expansion, obtaining a result consistent with the above to the precision shown.

(7) *Radiative corrections.* The factor $[1 + g_{v,b}]_{\text{EC}}$ is the EC radiative correction. Past work has either explicitly [36] or implicitly assumed that radiative corrections would affect the electron capture rate and the inverse neutrino capture cross section similarly, and

thus would be effectively included in calculations that extract an effective GT matrix element from electron capture, then use that amplitude in computing the inverse (ν_e, e^-) reaction. Sirlin [48] has pointed out that certain single-nucleon short-range contributions to radiative corrections are universal. But other contributions, notably bremsstrahlung, affect electron capture and neutrino reactions unequally, with the differences dependent on the Q value of the reaction [49]. When we evaluate the corresponding corrections for neutrino capture $[1 + g_{v,b}]_{(\nu,e)}$, we will obtain a ratio of radiative corrections that isolates the nonuniversal contribution, which we will then evaluate.

Collecting all of the results from this section and utilizing the 11.43 ± 0.03 d (1σ) half-life of ^{71}Ge we find

$$\omega = (7.019 \pm 0.037) \times 10^{-7}/s \quad (95\% \text{ C.L.})$$
$$= (8.122 \pm 0.122) \times 10^{-6} B_{\text{GT}}^{(\nu,e)}(\text{g.s.})\,[1 + g_{v,b}]_{\text{EC}}$$

and therefore

$$B_{\text{GT}}^{(\nu,e)}(\text{g.s.})[1 + g_{v,b}]_{\text{EC}} \equiv \tilde{B}_{\text{GT}}^{(\nu,e)}(\text{g.s.})$$
$$= 0.0864 \pm 0.0013 \quad (95\% \text{ C.L.}) \tag{13}$$

where the various uncertainties noted above have been combined in quadrature. The ground-state transition probability is conservatively known to a precision of about 1.5%: the primary motivation for the detailed discussion above was to establish this uncertainty. Our recommended best value of 0.0864 is consistent with most past estimates of this quantity, e.g., 0.087 [22], 0.0863 [36], and 0.0864 [50], though the agreement is a bit fortuitous, arising because differences in rate components cancel.

III. THE ^{71}Ga$(\nu_e, e^-)\,^{71}$Ge GROUND STATE CROSS SECTION

The ^{71}Ga(g.s.)$(\nu_e, e^-)\,^{71}$Ge(g.s.) neutrino capture cross section can be written in terms of $\tilde{B}_{\text{GT}}^{(\nu,e)}(\text{g.s.})$,

$$\sigma_{\text{g.s.}} = \frac{G_F^2 \cos^2\theta_C}{\pi} p_e E_e \, \mathcal{F}(Z_f, E_e) \, g_A^2 \, \tilde{B}_{\text{GT}}^{(\nu,e)}(\text{g.s.}) \frac{[1 + g_{v,b}]_{(\nu,e)}}{[1 + g_{v,b}]_{\text{EC}}} [1 + \epsilon_q]. \tag{14}$$

Nuclear recoil has been neglected as the target mass $M_T \gg E_e$. We evaluate the cross section for electron-capture neutrinos produced by ^{51}Cr and ^{37}Ar, for which the contributing lines are listed in Table I.

The neutrino energies E_ν and the corresponding branching ratios are computed from the respective Q values in ^{51}Cr and ^{37}Ar, 752.4 and 813.9 keV, the K-shell binding energies, 5.99 and 3.21 keV, the L-shell binding energies, 0.70 and 0.33 keV, the M-shell binding energies, 0.074 and 0.029 keV, the $K/L/M$ branching ratios of 0.891/0.094/0.016 and 0.902/0.0866/0.011, and the 9.93% branching ratio for ^{51}Cr to decay to the first excited $\frac{5}{2}^-$ state in ^{51}V at 321.1 keV

The various terms in Eq. (14) are

(1) *Kinematics.* The energy and three-momentum magnitude of the outgoing electron are denoted E_e and p_e, respectively. For the neutrino reactions of interest off ^{71}Ga,

$$E_e = E_\nu - Q_{\text{EC}} + m_e - 0.09 \text{ keV,}$$

where Q_{EC} in given in Eq. (2). We follow Bahcall [36] in including a very small 0.09 keV correction for the energy lost to electronic rearrangement, as the electron cloud adjusts to the nuclear charge change. For transitions to the $\frac{5}{2}^-$ (175 keV) and $\frac{3}{2}^-$ (500 keV) excited states in ^{71}Ge, the nuclear excitation energies would be added to Q_{EC}.

TABLE I. Neutrino source parameters and various correction factors that enter into the calculation of the cross section $\sigma_{\text{g.s.}}(\nu_e + {}^{71}\text{Ga} \rightarrow e^- + {}^{71}\text{Ge})$ for ${}^{51}\text{Cr}$ and ${}^{37}\text{Ar}$ neutrino sources. We report the energy of the incoming neutrino, E_ν, the corresponding neutrino branching ratio, and the energy of the final-state electron, E_e. $\mathcal{F}(Z_f, E_e)$ is the Coulomb factor of the electron, obtained by combining the various correction factors F_0, L_0, U, and S (see text). Finally, ϵ_q governs the strength of the forbidden corrections to the GT amplitude, and $[1 + g_{v,b}]_{(\nu,e)}/[1 + g_{v,b}]_{\text{EC}}$ measures the difference in radiative corrections that enter into the calculation of the respective cross sections for neutrino capture and the inverse process of electron capture.

Source	E_ν (MeV)	Branching	E_e (MeV)	F_0	L_0	U	S	$\mathcal{F}(Z_f, E_e)$	$1 + \epsilon_q$ (95% C.L.)	$\frac{[1+g_{v,b}]_{(\nu,e)}}{[1+g_{v,b}]_{\text{EC}}}$
${}^{51}\text{Cr}$	0.7524	0.0140	1.031	2.791	1.0034	0.9986	0.9920	2.774	1.0034 ± 0.0010	0.995
	0.7518	0.0842	1.030	2.791	1.0034	0.9986	0.9920	2.775	1.0034 ± 0.0010	0.995
	0.7465	0.8025	1.025	2.795	1.0035	0.9986	0.9920	2.779	1.0034 ± 0.0010	0.995
	0.4323	0.0015	0.711	3.335	1.0053	0.9985	0.9876	3.306	1.0017 ± 0.0005	0.997
	0.4317	0.0092	0.710	3.338	1.0053	0.9985	0.9876	3.309	1.0017 ± 0.0005	0.997
	0.4264	0.0886	0.705	3.360	1.0053	0.9985	0.9874	3.330	1.0017 ± 0.0005	0.997
${}^{37}\text{Ar}$	0.8138	0.0111	1.092	2.750	1.0031	0.9986	0.9925	2.734	1.0037 ± 0.0011	0.995
	0.8135	0.0866	1.092	2.750	1.0031	0.9986	0.9925	2.734	1.0037 ± 0.0011	0.995
	0.8107	0.9023	1.089	2.752	1.0031	0.9986	0.9925	2.736	1.0037 ± 0.0011	0.995

(2) *Coulomb corrections.* $\mathcal{F}(Z_f, E_e)$ corrects the phase space for the Coulomb distortion of the outgoing electron plane wave. Following [51], [52], and [53] this correction is decomposed as follows:

$$\mathcal{F}(Z_f, E_e) = F_0(Z_f, E_e)\, L_0(Z_f, E_e)\, U(Z_f, E_e)\, S(Z_f, E_e)$$

with

$$F_0(Z_f, E_e) = 4(2 p_e R_N)^{2(\gamma - 1)} e^{\pi y} \frac{|\Gamma(\gamma + iy)|^2}{[\Gamma(1 + 2\gamma)]^2},$$

$$\gamma \equiv \sqrt{1 - (\alpha Z_f)^2}, \quad y \equiv \alpha Z \frac{E_e}{p_e}.$$

F_0 is taken from the solution of the Dirac equation for an electron of momentum p_e in a point Coulomb potential generated by a charge Z_f, with $Z_f = 32$ here. This correction is kept finite by its evaluation at the nuclear surface, often taken to be $R_N \approx 1.2 A^{1/3}$ fm and interpreted as the edge of a nucleus of uniform density. We fix the ${}^{71}\text{Ge}$ rms charge radius to 4.05 fm, the average of the charge radii for ${}^{70}\text{Ge}$ and ${}^{72}\text{Ge}$, as measured in electron scattering [54], then use the relationship for a nucleus of uniform density to determine

$$R_N = \sqrt{\frac{5}{3}} \sqrt{\langle r^2 \rangle} = 5.23 \text{ fm} \approx 1.263 A^{1/3} \text{ fm}|_{A=71},$$

which we use in the evaluation. This initial estimate then must be corrected:

(1) L_0 accounts for most effects of the finite charge distribution. For a nucleus with a uniform density and thus a sharp surface at R_N, the Dirac solution can be continued to the origin by numerically integrating. We take L_0 from the tables of Behrens and Janecke [53], who performed the integration for $R_N = 1.2 A^{1/3}$ fm. We adjusted that result to account for the difference between this estimate of the rms charge radius and the experimental value used here, using Eq. (16) of [52] (or Eq. (2) of [55]).

(2) The factor $U(Z_f, E_e)$ represents the difference between the Coulomb distortion computed for a uniform charge distribution and that resulting from the use of a more realistic Fermi distribution with an equivalent rms radius. We use the parametrization of Wilkinson [51], also recently discussed in [52] [see Eqs. (29) and (30)].

(3) $S(Z_f, E_e)$ is a correction for atomic screening within the nuclear volume, which we take from Rose [56]. A comparison of various prescriptions for the atomic screening correction is presented in [52] (see Fig. 5 in this reference), showing generally good agreement, except for very low $E_e \lesssim 1.1 m_e$.

Table I gives the Coulomb factors $\mathcal{F}(Z_f, E_e)$ and the constituent corrections F_0, L_0, U, and S for ${}^{71}\text{Ga}(\nu_e, e^-)\,{}^{71}\text{Ge}$ for ${}^{51}\text{Cr}$ and ${}^{37}\text{Ar}$ neutrino sources.

(3) *Weak magnetism.* $[1 + \epsilon_q]$ corrects for the omission of forbidden contributions, dominated in this case by the interference between the GT amplitude and weak magnetism. After integrating over electron angles, the correction linear in weak magnetism takes on a form identical to Eq. (12),

$$\epsilon_q = \frac{2}{3 m_N g_A} \left(E_\nu + E_e - \frac{m_e^2}{E_e} \right)$$

$$\times \left[\mu_{T=1} + \frac{\langle \frac{3}{2}^- || \sum_{i=1}^A \boldsymbol{\ell}(i) \tau_-(i) || \frac{1}{2}^- \rangle}{\langle \frac{3}{2}^- || \sum_{i=1}^A \boldsymbol{\sigma}(i) \tau_-(i) || \frac{1}{2}^- \rangle_{\text{exp}}} \right],$$

(15)

apart from the kinematic factor. The resulting forbidden correction ϵ_q is shown in Table I. The 2σ uncertainty reflects the differences among the three SM estimates of the orbital matrix element, as discussed previously.

(4) *Nonuniversal radiative correction.* The ratio

$$\frac{[1 + g_{v,b}]_{(\nu,e)}}{[1 + g_{v,b}]_{\text{EC}}}$$

accounts for the difference between the radiative corrections [48] for neutrino absorption and those for electron capture [contained in $\tilde{B}_{GT}$(g.s.)]. While in a given low-energy weak nuclear process the radiative correction can be significant (a few percent [49]), it is frequently assumed [36] that these corrections affect inverse reactions (e^-, ν_e) and (ν_e, e^-) similarly, and thus are implicitly included when the (ν_e, e^-) nuclear transition matrix elements are determined from known electron-capture rates. Were this the case, the ratio above would be 1. However, while this universality assumption holds for charge-current reactions producing electrons/positrons only in the final or only in the initial state, Kurylov et al. [49] have shown that it is not preserved in the comparison between electron capture and (ν_e, e^-).

Kurylov et al. [49] evaluated the one-nucleon $W\gamma$-loop and bremsstrahlung contributions to the radiative corrections (Figs. 1(a) and 3 of [49]), finding that the bremsstrahlung contribution breaks the universality due to its dependence on the Q value. While the calculation treats the electron in (e^-, ν_e) as a free state, the results evaluated for $E_e \rightarrow m_e$ should approximate those needed for the weakly bound electrons of interest here. (The radiative corrections describe short-range loops and radiation associated with the strong Coulomb field near the nucleus. The bound electron wave function varies over atomic scales, not nuclear ones, providing justification for this assumption. In [57], similar issues are discussed in comparing muonium decay with free muon decay.)

The results shown in the last column of Table I were derived using Eqs. (4), (5), (51), and (52) of [49]. The difference in the one-nucleon/bremsstrahlung contributions to electron capture [implicitly absorbed into $\tilde{B}_{GT}$(g.s.)] and neutrino reactions yields a correction to the neutrino absorption cross section of $\approx 0.5\%$.

In addition to the effects discussed above, there are nucleus-dependent radiative corrections: contributions involving more than one nucleon (Fig. 1(b) of [49]) as well as the nuclear Green's function corrections to terms treated in leading order as one-nucleon contributions. Such corrections for the axial current have not yet been estimated and thus are not included here.

Cross sections. Combining all of the results above yields

$$\sigma_{\text{g.s.}} = \begin{cases} (5.39 \pm 0.08) \times 10^{-45} \text{ cm}^2, & {}^{51}\text{Cr}, \\ (6.45 \pm 0.10) \times 10^{-45} \text{ cm}^2, & {}^{37}\text{Ar} \end{cases} \quad (16)$$

at 95% C.L.

IV. EXCITED-STATE CONTRIBUTIONS

The excited-state contributions, which we will find increase the total cross section by about 6%, can also be extracted from experiment, specifically from forward-angle (p, n) scattering. However, past work has either failed to employ an appropriate effective interaction, or failed to propagate associated experimental and theoretical uncertainties, raising questions about the reliability of the extracted GT strengths. In this section we describe an improved extraction that yields both the needed transition strengths and reasonable estimates of their uncertainties.

Past work on excited-state contributions. The potential importance of excited-state contributions was noted by Kuzmin [58], when he proposed ^{71}Ga as a solar neutrino detector in 1966. In fact, one of the motivations for the ^{51}Cr and ^{37}Ar source experiments is that they populate the same excited states—the $5/2^-$ and $3/2^-$ states at 175 and 500 keV—that contribute to ^{7}Be solar neutrino capture (see Fig. 1).

In his 1978 Ga cross section study, Bahcall [59] used systematics to constrain the excited-state contributions, identifying transitions in neighboring nuclei that might be similar; that is, naively of a $2p_{3/2} \leftrightarrow 1f_{5/2}$ character. Bahcall identified nine $3/2^- \rightarrow 5/2^-$ transitions of known strength with $\log(ft)$ values ranging from 5.9 to 7.5, and consequently assigned $\log(ft) \gtrsim 6$ to the transition to the 175 keV state in ^{71}Ge. Similarly, he found eight $3/2^- \rightarrow 3/2^-$ transitions with $\log(ft)$ values ranging from 5.0 to 5.8, assigning $\log(ft) \gtrsim 5$ to the transitions to the 500 and 710 keV states. Using these bounds, Bahcall argued that the excited-state contribution to the ^{51}Cr absorption cross section would be $\lesssim 14.6\%$. But the potential fallibility of such arguments was pointed out in [22], as there are exceptions to these patterns in neighboring nuclei.

Alternatively, one might attempt a microscopic calculation of the strengths of the excited-state transitions. Indeed, SM calculations of the B_{GT} values for exciting the 175 and 500 keV states were performed early on by Baltz et al. [60] and by Mathews et al. [61]. But even today—as we will describe later—this is a dubious undertaking due to the weakness of these transitions. In the allowed approximation, the transition probabilities are proportional to the B_{GT} value,

$$B_{GT}(j_i\alpha_i \rightarrow j_f\alpha_f) = \frac{1}{2j_i + 1}|M_{GT}|^2$$

$$= \frac{1}{2j_i + 1}|\langle j_f\alpha_f||\hat{O}_{GT}^{J=1}||j_i\alpha_i\rangle|^2$$

$$\hat{O}_{GT}^{J=1} \equiv \sum_{j=1}^{A} \boldsymbol{\sigma}(j)\tau_+(j), \quad (17)$$

where $\boldsymbol{\sigma}$ is the Pauli spin matrix, τ_+ is the isospin raising operator, $||$ denotes a matrix element reduced in angular momentum, and $j_i\alpha_i$ and $j_f\alpha_f$ denote the quantum numbers of the initial and final states, respectively, with the angular momentum j made explicit. From the known EC rate for ^{71}Ge and from the lower bounds Bahcall used for the transitions to the 175 and 500 keV levels, one finds

$$B_{GT}({}^{71}\text{Ga g.s.} \rightarrow {}^{71}\text{Ge 175 keV}) \lesssim 0.004,$$

$$B_{GT}({}^{71}\text{Ga g.s.} \rightarrow {}^{71}\text{Ge 500 keV}) \lesssim 0.04, \quad (18)$$

values smaller than the ground-state B_{GT} value of Eq. (13). As the total B_{GT} strength, summed over all final states, is given approximately by the Ikeda sum rule $3(N - Z) = 27$ [62], we see that the transitions to the $5/2^-$ and $3/2^-$ states exhaust less than $\approx 0.01\%$ and 0.1% of the sum-rule strength, respectively. Consequently, one expects calculations to be sensitive to wave-function details, including the interactions

used, the adopted SM spaces, etc. A weak transition typically indicates substantial interferences among the individual amplitudes in the transition density matrix. Indeed, early attempts to estimate the needed excited-state contributions to the cross section, using the SM [60,61], schematic effective interactions, and truncated model spaces, yielded results that varied by orders of magnitude, depending on the specific simplifications adopted.

Here we make use of the full power of the modern SM—carefully tuned interactions like those discussed in the previous section, and the ability to treat all Slater determinants in the $2p_{3/2} 1f_{5/2} 2p_{1/2} 1g_{9/2}$ shell—but only to estimate corrections that typically alter results at the level of $\lesssim 10\%$. Apart from these corrections, the needed weak GT strengths are extracted from experiment.

Charge-exchange reactions. The possibility that excited-state GT strength could be measured through surrogate reactions, (p, n) or $({}^3\text{He}, t)$, generated significant interest in the solar neutrino community. The approximate proportionality between medium-energy forward-angle (p, n) cross sections and nuclear B_{GT} profiles is well established [63]. This method was applied to the ${}^{71}\text{Ga}$ transitions of interest by Krofcheck *et al.* [64]. From (p, n) measurements at 120 and 200 MeV they deduced

$$B_{\text{GT}}^{(p,n)}({}^{71}\text{Ga g.s.} \rightarrow {}^{71}\text{Ge 175 keV}) \lesssim 0.005,$$
$$B_{\text{GT}}^{(p,n)}({}^{71}\text{Ga g.s.} \rightarrow {}^{71}\text{Ge 500 keV}) = 0.011 \pm 0.002,$$
$$(19)$$

results qualitatively consistent with Bahcall's expectations based on systematics. However, the use of this method in the case of weak transitions can be problematic, as described in [22,23]. Here we extend these previous analyses with the goal of better quantifying the excited-state contributions to the neutrino absorption cross section.

The same transitions were studied using $({}^3\text{He}, t)$ at 420 MeV [65]. This method can achieve higher resolution, but has been applied less frequently to the light nuclei we will later use to test the reliability of charge-exchange mappings of Gamow-Teller strength. The results are

$$B_{\text{GT}}^{(p,n)}({}^{71}\text{Ga g.s.} \rightarrow {}^{71}\text{Ge 175 keV}) = 0.0034 \pm 0.0026,$$
$$B_{\text{GT}}^{(p,n)}({}^{71}\text{Ga g.s.} \rightarrow {}^{71}\text{Ge 500 keV}) = 0.0176 \pm 0.0014.$$
$$(20)$$

As the tension between Eqs. (19) and (20) for the transition to the $\frac{3}{2}^-$ state exceeds 3σ, we will treat the two data sets separately, rather than combining them.

Effective operators. The work in [22,23] exploited the empirical observation [66] that the effective operator for forward-angle (p, n) scattering includes a subdominant contribution from a tensor operator $\hat{O}_{\text{T}}^{J=1}$,

$$M^{(p,n)} \equiv M_{\text{GT}} + \delta M_{\text{T}}, \quad M_{\text{T}} \equiv \langle j_f \alpha_f || \hat{O}_{\text{T}}^{J=1} || j_i \alpha_i \rangle,$$

$$\hat{O}_{\text{T}}^{J=1} = \sqrt{8\pi} \sum_{j=1}^{A} [Y_2(\Omega_j) \otimes \boldsymbol{\sigma}(j)]_{J=1} \tau_+(j), \quad (21)$$

where $\delta \approx 0.1$, so that

$$B_{\text{GT}}^{(p,n)} = \frac{1}{2j_i + 1} |\langle j_f \alpha_f || M^{(p,n)} || j_i \alpha_i \rangle|^2. \quad (22)$$

The need for the tensor correction in forward-angle scattering, where the momentum transfer is minimal and thus the interactions can occur at long range, should not be a surprise: the central part of the one-pion-exchange potential generates a target response proportional to M_{GT} while the tensor part generates M_{T}. In cases where M_{GT} is weak but M_{T} is strong, $M^{(p,n)}$ will be an unreliable probe of B_{GT} strengths. An example where this would be the case is an ℓ-forbidden $M1$ transition, where the dominant amplitude links orbitals with the quantum numbers $[n, \ell, j + \frac{1}{2}]$ and $[n - 1, \ell + 2, j = \ell + \frac{3}{2}]$. Such transitions are often found at low energy in nuclear spectra, as a consequence of an approximate pseudospin symmetry [67]. A candidate ℓ-forbidden transition [22] is ${}^{71}\text{Ga}(3/2^-) \rightarrow {}^{71}\text{Ge}(5/2^-)$, which would be described in the naive SM as $1f_{5/2}$ (n hole) $\rightarrow 2p_{3/2}$ (p particle). State-of-the-art SM studies performed here and in another recent study [68] show that the transition density matrix does have an important ℓ-forbidden component.

Estimating the size of the tensor contribution. The analysis in [22] estimated δ by examining GT transitions in $1p$- and $2s1d$-shell nuclei, but did not evaluate the experimental and theoretical errors in the determination, nor how they would propagate into an estimate of δ and consequently the ${}^{71}\text{Ga}$ excited-state cross section. Given the BEST anomaly, it is now important to do so. The data examined in [22] were sensibly chosen, involving mirror transitions where β decay and (p, n) transition strengths were both available from experiment, including transitions near closed shells where levels are well separated and thus their SM wave functions less sensitive to small changes in effective interactions. However, we have made some changes in the data set, reflecting new information that has become available. We also assess theoretical uncertainties by employing several available effective interactions in computing M_{T}: to relate $M^{(p,n)}$ and M_{GT}, $|M_{\text{T}}|$ and the sign of $M_{\text{T}}/M_{\text{GT}}$ must be computed.

The data we use in determining δ are given in Table II (compare to Table 1 of [22]) and consist primarily of isospin mirror transitions where both (p, n) and β-decay strengths are known. Eight of these cases are taken from the compilation of $B_{\text{GT}}^{(p,n)}$ of [66]. To convert the proportionality between (p, n) scattering and β decay into an equivalence, a normalization must be introduced. Often this is done by using, for each target nucleus, a strong β decay transition, which can still be problematic if there are corrections due to $\hat{O}_{\text{T}}^{J=1}$ that affect normalizing transitions in differential ways. The study of [66] instead computed normalizing cross sections in the distorted-wave impulse approximation, employing a phenomenological interaction fitted to a large body of data. This then avoids the issue of nucleus-by-nucleus normalization systematics.

Here we make two modifications in the compiled $B_{\text{GT}}^{(p,n)}$ values. The first is a reduction by a factor of $(1.251/1.276)^2$ to account for the current value of g_A. The second addresses the absence of experimental errors on the compiled [66] BGT values. In previous work a value for δ was obtained by a

TABLE II. Weak transitions and their beta decay and (p, n) amplitudes deduced from experiment. The sign of M_{GT} has been taken as positive. M_T and its sign relative to M_{GT} have been taken from theory, except for the case of the sign of ^{32}S (see text).

Reaction[a]	$\log(ft)$[b]	$(2J_i + 1)B_{GT}$	$\frac{B_{GT}^{(p,n)}}{B_{GT}}$	M_{GT}	$M^{(p,n)}$	M_T[c]	$\frac{M_T}{M^{(p,n)}}$
^{13}C$(\frac{1}{2}^-) \leftrightarrow {}^{13}N(\frac{1}{2}^-)$	3.6648(5)	0.404 ± 0.002	1.85 ± 0.22	0.636 ± 0.002	0.87 ± 0.05	2.8 ± 0.3	3.2
$\left.\begin{array}{l}{}^{14}\text{C}(0^+)\\{}^{14}\text{O}(0^+)\end{array}\right\} \to {}^{14}N(1^+\ 3.95\ \text{MeV})$	3.131(17)	2.79 ± 0.11	0.97 ± 0.12	1.67 ± 0.03	1.65 ± 0.10	0.086 ± 0.009	0.052
^{15}N$(\frac{1}{2}^-) \leftrightarrow {}^{15}O(\frac{1}{2}^-)$	3.6377(8)	0.509 ± 0.003	2.04 ± 0.24	0.713 ± 0.002	1.02 ± 0.06	3.3 ± 0.3	3.2
^{17}O$(\frac{5}{2}^+) \leftrightarrow {}^{17}F(\frac{5}{2}^+)$	3.3562(5)	6.280 ± 0.011	0.91 ± 0.11	2.506 ± 0.002	2.39 ± 0.14	1.7 ± 0.2	0.69
^{18}O$(0^+) \leftrightarrow {}^{18}F(1^+)$	3.5700(19)	3.045 ± 0.013	1.12 ± 0.13	1.745 ± 0.003	1.84 ± 0.11	-0.04 ± 0.03	-0.02
$\left.\begin{array}{l}{}^{18}\text{O}(0^+)\\{}^{18}\text{Ne}(0^+)\end{array}\right\} \to {}^{18}F(1^+\ 1.70\ \text{MeV})$	4.470(15)	0.128 ± 0.004	1.33 ± 0.17	0.358 ± 0.006	0.41 ± 0.025	0.8 ± 0.3	2
^{19}F$(\frac{1}{2}^+) \leftrightarrow {}^{19}Ne(\frac{1}{2}^+)$	3.2329(24)	3.184 ± 0.024	1.29 ± 0.15	1.784 ± 0.007	2.02 ± 0.12	0.08 ± 0.03	0.04
^{19}F$(\frac{1}{2}^+) \leftrightarrow {}^{19}Ne(\frac{3}{2}^+\ 1.55\ \text{MeV})$	5.71(5)	0.0294 ± 0.0034	2.65 ± 0.41	0.172 ± 0.010	0.279 ± 0.014	1.41 ± 0.04	5.06
$\left.\begin{array}{l}{}^{26}\text{Mg}(0^+)\\{}^{26}\text{Si}(0^+)\end{array}\right\} \to {}^{26}Al(1^+\ 1.06\ \text{MeV})$	3.550(11)	1.063 ± 0.027	1.03 ± 0.13	1.031 ± 0.013	1.05 ± 0.06	1.20 ± 0.08	1.14
^{32}S$(0^+) \leftrightarrow {}^{32}Cl(1^+)$	6.74(18)	0.0021 ± 0.0009	$6.9^{+7.3}_{-4.1}$	0.046 ± 0.010	0.116 ± 0.043	0.99 ± 0.05	8.6
^{39}K$(\frac{3}{2}^+) \leftrightarrow {}^{39}Ca(\frac{3}{2}^+)$	3.6326(10)	1.060 ± 0.008	1.41 ± 0.17	1.030 ± 0.004	1.22 ± 0.07	3.1 ± 0.3	2.5

[a]Transitions are between ground states unless otherwise specified.

[b]Taken from the ENSDF compilations.

[c]$2s1d$-shell uncertainties (excluding ^{39}K $\to {}^{39}$Ca) correspond to the 1σ spread of matrix elements computed from the USDA, USDB [75], and Brown-Wildenthal [74] interactions. All other M_T uncertainties are assumed to be 10%.

simple fit, which weights all data points equally and precludes a realistic estimate of the uncertainty for the derived δ. As discussed below, we now include several new transitions in our analysis where uncertainties are available. For the transitions we retain from the tabulation of [66], we have estimated uncertainties using [69], which [66] references for experimental details. The uncertainties tabulated there include the efficiency determination ($\pm 8\%$), beam normalization ($\pm 5\%$), neutron attenuation ($\pm 5\%$), counting statistics ($\pm 3\%$), and background subtractions ($\pm 5\%$). Combining these in quadrature yields an estimated $\pm 12\%$ uncertainty, which we adopt for all of the stronger transitions in Table II. (Reference [69] also includes a correction for target water absorption, but that correction addresses an issue specific to one target.) The uncertainty inherent in (p, n) mappings of B_{GT} strength has been frequently discussed, with most estimates in range of 10—20% [70]. Our choice of 12% is consistent with this range.

Two additional transitions used in [22,23], ^{32}S$(0^+) \leftrightarrow {}^{32}Cl(1^+)$ and ^{39}K$(\frac{3}{2}^+) \leftrightarrow {}^{39}Cl(\frac{1}{2}^+)$, are candidate ℓ-forbidden $M1$ transitions sensitive to the tensor amplitude. One expects both to be dominated by the transition density $2s_{1/2} \leftrightarrow 1d_{3/2}$. The ^{39}K $M^{(p,n)}$ given in [22] was extracted from raw (p, n) cross sections as an order-of-magnitude estimate: there is no experimentally extracted $B_{GT}^{(p,n)}$ value. No meaningful error can be assigned to this very weak transition, so it is not included here. The ^{32}S transition was reconsidered in [71], where a large uncertainty was assigned, which we adopt for our analysis. The impact of this transition on the current analysis is greatly diminished by the size of that uncertainty.

We also include two $2s1d$-shell transitions not considered in earlier analyses, one a recent result for ^{26}Mg$(0^+) \to {}^{26}$Al$(1^+, 1.70\ \text{MeV})$, obtained from $(^3\text{He}, t)$. While this result

was normalized to the ^{26}Al ground state β decay rate, the unusually weak tensor contribution we predict for the normalizing transition ($\lesssim 1\%$) allows us to accept this result. The second is ^{19}F$(\frac{1}{2}^+) \to {}^{19}Ne(\frac{3}{2}^+, 1.55\ \text{MeV})$, a transition that is strongly ℓ-forbidden, according to the shell model, and thus potentially quite sensitive to $\hat{O}_T^{J=1}$.

The data displayed in Table II include β decay $\log(ft)$ values taken from the ENSDF data files [72], from which we determine M_{GT} and its uncertainty, and calculations of M_T; one needs both the magnitude and sign of this quantity relative to M_{GT}. In nine of the tabulated cases the shell-model calculations we perform (see below) yield a positive relative sign, and thus a positive δ to account for the observed enhancement in $|M^{(p,n)}|/|M_{GT}|$. There are two exceptions: The three shell model calculations we performed for ^{18}O$(0^+) \to {}^{18}$F(1^+) all predict a negative M_T, but with a magnitude so small that it has no impact on our study. For ^{19}F$(\frac{1}{2}^+) \to {}^{19}Ne(\frac{3}{2}^+, 1.55\ \text{MeV})$, the shell model calculations disagree on the sign, and all underestimate the already quite suppressed M_{GT} derived from experiment. We have assumed constructive interference as this is indicated by experiment and is consistent with the calculation that best reproduces the known value of $|M_{GT}|$ (the USDA shell model result described below).

Our shell-model calculations of M_T were performed with the Cohen and Kurath [73] interaction in the $1p$ shell and the Brown-Wildenthal [74] and USDA/USDB [75] interactions in the $2s1d$ shell. The availability of three $2s1d$ interactions that each do well in reproducing $2s1d$ spectroscopy provides an opportunity to assess theory uncertainties. The $2s1d$-shell values in the table are the means and standard deviations of the three calculations. There is excellent consistency, typically at the level of 10%. Even by eye, there is clearly a strong correlation between the cases in Table II where $|M_T|/|M_{GT}|$ is large and those where the experimental ratio $|B_{GT}^{(p,n)}|/|B_{GT}|$ is sig-

nificantly above 1. In the four cases where the $|B_{GT}^{(p,n)}|/|B_{GT}|$ exceeds 1.4, $|M_T|/|M_{GT}|$ ranges from 2.5 to 8.6.

Extracting M_{GT} from (p, n) cross sections. We use these results to test whether the inclusion of the tensor operator in Eq. (21) improves the agreement between $M^{(p,n)}$ and M_{GT}. Evaluating the χ^2 per degree of freedom with and without M_T yields

$$\frac{1}{11} \sum_{i=1}^{A} \frac{[M_{GT}(i) - M^{(p,n)}(i)]^2}{\sigma(i)^2} \approx 9.4,$$

$$\frac{1}{10} \sum_{i=1}^{A} \frac{(M_{GT}(i) + \delta M_T(i) - M^{(p,n)}(i))^2}{\sigma(i)^2} \approx 1.0, \quad (23)$$

where $\delta = 0.076$, and $\sigma(i)$ is generated by combining uncertainties for $M^{(p,n)}$ and M_{GT} in quadrature. While a simple proportionality between B_{GT} strength and (p, n) scattering for individual states is not supported by the data, the proportionality is restored with the introduction of M_T to a level consistent with the statistical fluctuations of the data. The variation around the minimum to achieve a unit change in the total χ^2 yields the estimate $\delta = 0.076 \pm 0.008$ at 1σ.

The analysis can also be done by examining each target separately: this approach has advantages in understanding the relationship of the current work to that of [22,23]. For each target i we determine a probability distribution for $\delta(i)$ from the relation $M_{GT}(i) + \delta(i)M_T(i) - M^{(p,n)}(i) = 0$, treating the errors on $M_{GT}(i)$, $M_T(i)$, and $M^{(p,n)}(i)$ as Gaussian with the uncertainties listed in Table II. The convolution was done by discretizing the probability distributions in bins, and independently by Monte Carlo, and the results cross-checked to verify their numerical accuracy. The theory errors on M_T (see Table II) were computed from the standard deviations of the SM results in the cases where multiple effective interactions were explored; in the five cases where only a single shell-model calculation was done, we assigned an uncertainty of 10%, a value typical of the other cases. (In the simple χ^2 fit described previously, we used the best values for the M_T, neglecting the uncertainties.)

The resulting probability distributions for the $\delta(i)$, while not exactly Gaussian, turn out to be nearly so in all cases. The equivalent Gaussian means and standard deviations are given in Table III. These results can then be combined to form the overall uncertainty-weighted mean and standard deviation, $\delta = 0.074 \pm 0.008$ (1σ), a result nearly identical to that obtained more simply from the χ^2. This is our final result for δ.

In this fit, the result is dominated by four transitions, from ^{13}C, ^{15}N, ^{39}K, and ^{19}F to the excited state, which are four of the five cases where M_T exceeds M_{GT} by factors $\gtrsim$ 2.5. If only these four transitions are retained, one obtains $\delta = 0.078 \pm 0.009$. The other seven constraints have a minimal effect, shifting the mean by $\approx$5% and improving the precision by only $\approx$6%. This reflects the fact that in computing the weighted mean and uncertainty, the contributions of these seven are diluted by their low weights, $w_i = 1/\sigma_i^2$, for the σ_i of Table III. Thus it is somewhat fortuitous that earlier work [22,23] in which central values were fit, thereby weight-

TABLE III. The Gaussian means $\bar{\delta}_i$ and standard deviations σ_i for the distributions δ_i obtained from each of the reactions. The weighted combination of these results yields $\delta = 0.074 \pm 0.008$ (1σ).

Reaction	$\bar{\delta}_i$	σ_i
^{13}C$(\frac{1}{2}^-) \leftrightarrow$ ^{13}N$(\frac{1}{2}^-)$	0.082	0.020
$\left.\begin{array}{l} ^{14}\text{C}(0^+) \\ ^{14}\text{O}(0^+) \end{array}\right\} \rightarrow$ ^{14}N$(1^+$ 3.95 MeV$)$	-0.24	1.21
^{15}N$(\frac{1}{2}^-) \leftrightarrow$ ^{15}O$(\frac{1}{2}^-)$	0.093	0.021
^{17}O$(\frac{5}{2}^+) \leftrightarrow$ ^{17}F$(\frac{5}{2}^+)$	-0.070	0.085
^{18}O$(0^+) \leftrightarrow$ ^{18}F(1^+)	-1.59	2.48
$\left.\begin{array}{l} ^{18}\text{O}(0^+) \\ ^{18}\text{Ne}(0^+) \end{array}\right\} \rightarrow$ ^{18}F$(1^+$ 1.70 MeV$)$	0.063	0.040
^{19}F$(\frac{1}{2}^+) \leftrightarrow$ ^{19}Ne$(\frac{1}{2}^+)$	2.69	1.80
^{19}F$(\frac{1}{2}^+) \leftrightarrow$ ^{19}Ne$(\frac{3}{2}^+$ 1.55 MeV$)$	0.076	0.012
$\left.\begin{array}{l} ^{26}\text{Mg}(0^+) \\ ^{26}\text{Si}(0^+) \end{array}\right\} \rightarrow$ ^{26}Al$(1^+$ 1.06 MeV$)$	0.015	0.051
^{32}S$(0^+) \leftrightarrow$ ^{32}Cl(1^+)	0.070	0.045
^{39}K$(\frac{3}{2}^+) \leftrightarrow$ ^{39}Ca$(\frac{3}{2}^+)$	0.061	0.023

ing each target equally, gave results consistent with the range determined here. (The results from [22,23] are $\delta = 0.096$ and 0.069 for the $1p$ and $2s1d$ shells, respectively.)

These results and their relevance to the ^{71}Ga(ν_e, e^-) ^{71}Ge cross section are apparent from Fig. 2. The agreement between the (p, n) amplitude $|M^{(p,n)}|$ and $|M_{GT}|$, which is excellent for transitions with strong B_{GT} values, systematically deteriorates as B_{GT} is reduced. But this deterioration is corrected by the inclusion of M_T. The shaded region at small B_{GT} is that relevant for the two ^{71}Ga excited-state transitions: based on the trends apparent from the figure, the interpretation of (p, n) data for these transitions would not be reliable unless the effects of M_T are treated.

From Fig. 2 one sees that a fixed δ brings the (p, n) results into accord with known Gamow-Teller strengths throughout the $1p$ and $2s1d$ shells. The absence of any evident dependence on mass number justifies the use of the same δ in our ^{71}Ga cross section work. It would be helpful to verify this assumption by extending the results of Fig. 2 into the $2p_{3/2}1f_{5/2}2p_{1/2}1g_{9/2}$ shell. Obstacles to doing this successfully include the absence of an experimental compilation for heavier nuclei analogous to that of [66], fewer opportunities to exploit isospin mirror transitions (which play a major role in the analysis presented here), and the theory challenge of evaluating the tensor amplitudes in systems with higher level densities and consequently more delicate level mixing.

V. RECOMMENDED EXCITED-STATE B_{GT} VALUES

With $\delta = 0.074 \pm 0.008$ (1σ) determined, we can now extract from (p, n) measurements best values and estimated uncertainties for M_{GT} for the two excited-state contributions to ^{71}Ga(ν_e, e^-) ^{71}Ge, using

$$M^{(p,n)} = M_{GT} + \delta M_T.$$

This requires us to compute the magnitude and relative sign of M_T. The theory task is more challenging than that of the previous section because the effective interactions available
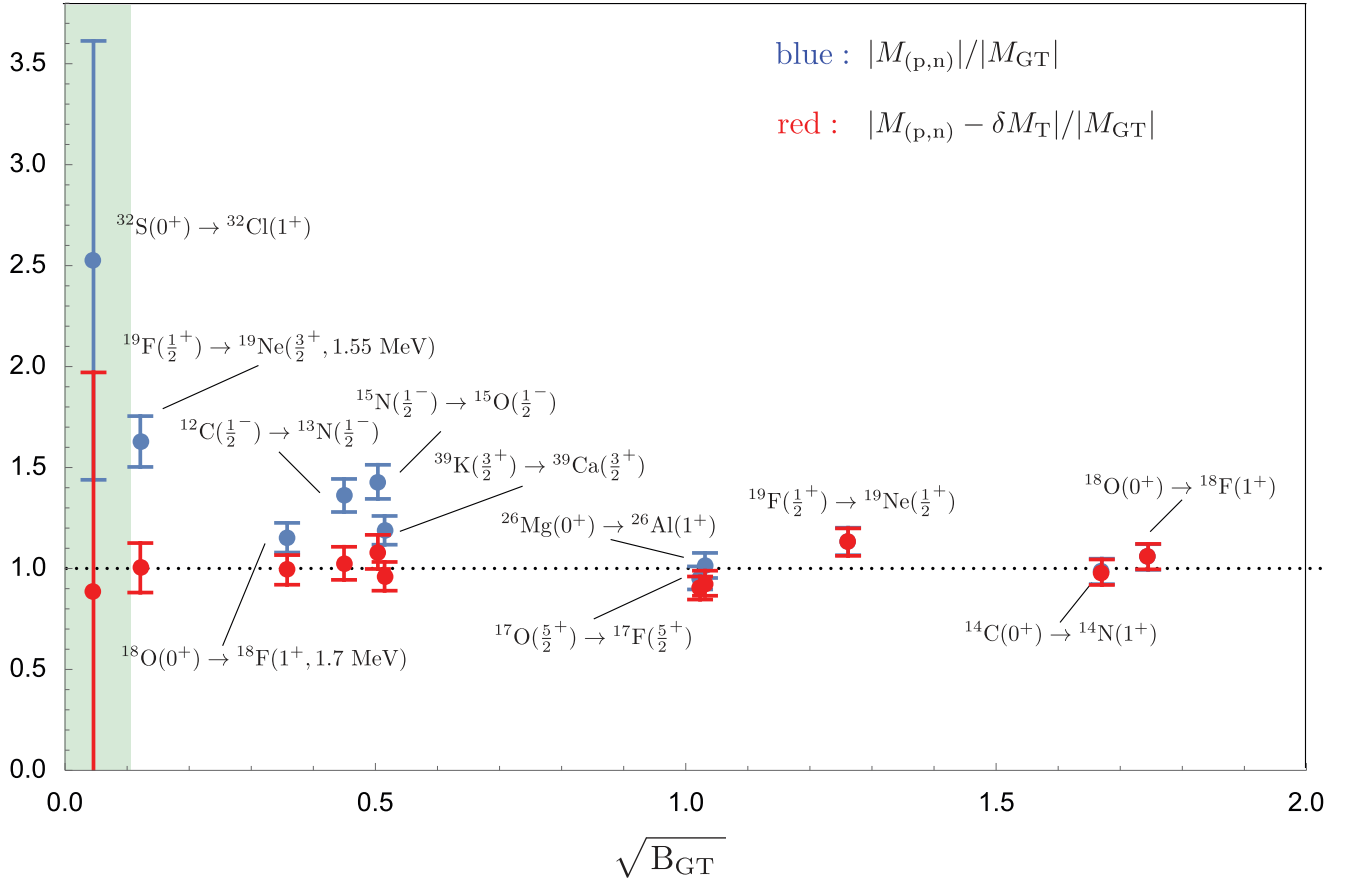
FIG. 2. In blue: correspondence between the (p, n) amplitude $|M^{(p,n)}|$ and the β-decay amplitude $|M_{\rm GT}|$ is excellent when $B_{\rm GT}$ is strong, but deteriorates for weaker $B_{\rm GT}$. In red: when the effects of $M_{\rm T}$ are included in the relationship between $M_{\rm GT}$ from $M^{(p,n)}$, such discrepancies disappear. The two excited states that contribute to the BEST cross section have weak transition strengths that would place them in the shaded region, where large tensor contributions would be anticipated.

for the relevant shell-model space, $2p_{3/2}1f_{5/2}2p_{1/2}1g_{9/2}$, are known to be less successful in their spectroscopic predictions. These nuclear physics uncertainties should be reflected in the range of the predicted $M_{\rm T}$.

As was done in the $2s1d$ shell, calculations were performed with three well-tested interactions, GCN2850 [37],

jj44b [38], and JUN45 [39], including all m-scheme Slater determinants that can be formed in the valence space ($\approx 10^8$ basis states). The results are shown in Table IV. There is reasonable agreement among these calculations on magnitudes and signs, and, as before, we combine the results to obtain best values and 1σ ranges. The combined results are

TABLE IV. ^{71}Ga SM transitions matrix elements evaluated for each of three interactions. For transitions to the two excited states in ^{71}Ge, the predicted values and 1σ ranges for $M_{\rm T}$ are used in the extraction of $|M_{\rm GT}|$ from forward-angle (p, n) measurements. We include the SM values for $M_{\rm GT}$, denoted $M_{\rm GT}^{\rm SM}$, to illustrate that SM GT transition strengths vary considerably for weak transitions, even when highly tuned effective interactions are employed. For this reason $M_{\rm GT}$ is extracted from experiment, not from theory. Theory is used only in estimating $M_{\rm T}$, a correction in the (p, n) analysis that generically enters at the level of $\approx 8\%$. This strategy dilutes the impact of nuclear structure uncertainties.

Transition	Interaction	$M_{\rm GT}^{\rm SM}$	$M_{\rm T}$	$\overline{M}_{\rm T}$
$\frac{3}{2}^- \to \frac{1}{2}^-$ (g.s.)	JUN45	0.791	-0.516	
	GCN2850	0.361	-0.320	-0.37 ± 0.13
	jj44b	0.290	-0.283	
$\frac{3}{2}^- \to \frac{5}{2}^-$ (175 keV)	JUN45	0.145	-0.764	
	GCN2850	0.159	-0.410	-0.50 ± 0.24
	jj44b	0.264	-0.311	
$\frac{3}{2}^- \to \frac{3}{2}^-$ (500 keV)	JUN45	0.096	0.062	
	GCN2850	0.196	-0.178	-0.088 ± 0.13
	jj44b	0.505	-0.148	

denoted $\overline{M}_{\mathrm{GT}}$ and $\overline{M}_{\mathrm{T}}$. The results for $\overline{M}_{\mathrm{T}}$—its magnitude and sign relative to M_{GT}—are needed in the analysis below. An immediate cross-check on the nuclear structure comes from the known B_{GT} value derived from the ^{71}Ge electron capture rate, $B_{\mathrm{GT}} = 0.0864 \pm 0.0013$ (2σ), from which one finds $M_{\mathrm{GT}} = 0.588 \pm 0.002$ (1σ), in good agreement with the shell-model result, $\overline{M}_{\mathrm{GT}} = 0.48 \pm 0.27$ (1σ). After we extract the M_{GT}'s from the (p, n) results, we will be able to make similar comparisons for the excited states. Note that the shell model indicates largely destructive interference between the M_{GT} and M_{T} amplitudes for the three transitions of interest.

Analysis for Krofcheck et al. The forward-angle (p, n) scattering results of Krofcheck *et al.* [64] for exciting the ^{71}Ge ground-state $(\frac{1}{2}^-)$, 175 keV $(\frac{5}{2}^-)$, and 500 keV $(\frac{3}{2}^-)$ levels yield $B_{\mathrm{GT}}^{(p,n)} = 0.089 \pm 0.007$, <0.005, and 0.011 ± 0.002, respectively. These results were normalized to the analog transition using an energy-dependent coefficient relating $B_{\mathrm{GT}}^{(p,n)}$ to cross sections. As we are concerned with states in a narrow energy band, we can avoid any issues with this choice by forming the ratios

$$\frac{B_{\mathrm{GT}}^{(p,n)}\left(\frac{5}{2}^-\right)}{B_{\mathrm{GT}}^{(p,n)}(\mathrm{g.s.})} \equiv \frac{\left|M_{\mathrm{GT}}\left(\frac{5}{2}^-\right) + \delta\overline{M}_{\mathrm{T}}\left(\frac{5}{2}^-\right)\right|^2}{\left|M_{\mathrm{GT}}(\mathrm{g.s.}) + \delta\overline{M}_{\mathrm{T}}(\mathrm{g.s.})\right|^2}$$
$$< 0.06 \quad (68\% \text{ C.L.}), \tag{24}$$

$$\frac{B_{\mathrm{GT}}^{(p,n)}\left(\frac{3}{2}^-\right)}{B_{\mathrm{GT}}^{(p,n)}(\mathrm{g.s.})} \equiv \frac{\left|M_{\mathrm{GT}}\left(\frac{3}{2}^-\right) + \delta\overline{M}_{\mathrm{T}}\left(\frac{3}{2}^-\right)\right|^2}{\left|M_{\mathrm{GT}}(\mathrm{g.s.}) + \delta\overline{M}_{\mathrm{T}}(\mathrm{g.s.})\right|^2}$$
$$= 0.124 \pm 0.024 \quad (68\% \text{ C.L.}). \tag{25}$$

We first consider the transition to the $\frac{3}{2}^-$ state. Because the electron capture M_{GT} is so precisely known, we use the central value in the analysis below. We insert the values for the two tensor matrix elements M_{T} and δ, including their uncertainties. We take the (dominant) sign of M_{T} relative to M_{GT} from theory. We assume all distributions are normal (Gaussian), described by the specified standard deviations, then compute the associated distribution for the needed B_{GT} ratio, which we find is also well represented by a normal distribution. This yields

$$\frac{B_{\mathrm{GT}}\left(\frac{3}{2}^-\right)}{B_{\mathrm{GT}}(\mathrm{g.s.})} \equiv \frac{\left|M_{\mathrm{GT}}\left(\frac{3}{2}^-\right)\right|^2}{|M_{\mathrm{GT}}(\mathrm{g.s.})|^2} = 0.121 \pm 0.026 \quad (68\% \text{ C.L.}).$$
$$\tag{26}$$

The tensor corrections have little impact, shifting the numerator and denominator similarly, by 3.2% and 4.7% respectively, with these shifts largely canceling when the ratio is formed. The central value obtained for $|M_{\mathrm{GT}}(\frac{3}{2}^-)| \approx 0.20$ is consistent with the shell-model range in Table IV, 0.27 ± 0.21.

In our shell-model calculations the density matrices for the transition to the 175 keV $\frac{5}{2}^-$ state are dominated by the the ℓ-forbidden amplitude $2p_{3/2} \to 1f_{5/2}$, which reaches single-particle strength in the case of the JUN45 calculation. This is the reason for the strength of M_{T} and the weakness of M_{GT} in the shell-model studies of Table IV, and consequently $\overline{M}_{\mathrm{T}}/\overline{M}_{\mathrm{GT}} \approx -2.6$. The destructive interference allows for a larger $|M_{\mathrm{GT}}|$ than would be the case if the tensor contributions

to (p, n) scattering were ignored. As was done for the 500 keV state, we take into account the uncertainties on the various quantities by integrating over the probability distributions of each input variable, taking the ranges of the $\overline{M}_{\mathrm{T}}$ from the results of Table IV. In this calculation we interpret the experimental bound given in the first of Eqs. (25) as a measurement of 0 with a one-sided normal distribution described by $\sigma = 0.06$. We find

$$\left|M_{\mathrm{GT}}\left(\frac{5}{2}^-\right)\right| \lesssim \begin{cases} 0.18, & 68\% \text{ C.L.}, \\ 0.24, & 95\% \text{ C.L.}, \end{cases}$$

$$\frac{B_{\mathrm{GT}}\left(\frac{5}{2}^-\right)}{B_{\mathrm{GT}}(\mathrm{g.s.})} \lesssim \begin{cases} 0.089, & 68\% \text{ C.L.}, \\ 0.160, & 95\% \text{ C.L.} \end{cases} \tag{27}$$

Analysis for Frekers et al.. We repeat the analysis for the Frekers *et al.* [65] data, as the use of the same effective operator for $(^3\mathrm{He}, t)$ has support from both theory and experiment [76], while noting that a separate derivation of δ based on data like those of Table II has not been done for this reaction. We again form the ratios

$$\frac{B_{\mathrm{GT}}^{(^3\mathrm{He},t)}\left(\frac{5}{2}^-\right)}{B_{\mathrm{GT}}^{(^3\mathrm{He},t)}(\mathrm{g.s.})} \equiv \frac{\left|M_{\mathrm{GT}}\left(\frac{5}{2}^-\right) + \delta\overline{M}_{\mathrm{T}}\left(\frac{5}{2}^-\right)\right|^2}{\left|M_{\mathrm{GT}}(\mathrm{g.s.}) + \delta\overline{M}_{\mathrm{T}}(\mathrm{g.s.})\right|^2}$$
$$= 0.040 \pm 0.031 \quad (68\% \text{ C.L.}),$$

$$\frac{B_{\mathrm{GT}}^{(^3\mathrm{He},t)}\left(\frac{3}{2}^-\right)}{B_{\mathrm{GT}}^{(^3\mathrm{He},t)}(\mathrm{g.s.})} \equiv \frac{\left|M_{\mathrm{GT}}\left(\frac{3}{2}^-\right) + \delta\overline{M}_{\mathrm{T}}\left(\frac{3}{2}^-\right)\right|^2}{\left|M_{\mathrm{GT}}(\mathrm{g.s.}) + \delta\overline{M}_{\mathrm{T}}(\mathrm{g.s.})\right|^2}$$
$$= 0.207 \pm 0.019 \quad (68\% \text{ C.L.}). \tag{28}$$

The calculation for the 500 keV $\frac{3}{2}^-$ excited state state proceeds as before, taking into account the values and uncertainties for the two tensor matrix elements M_{T} and δ, and taking the relative signs of the M_{T} from theory. This yields

$$\frac{B_{\mathrm{GT}}\left(\frac{3}{2}^-\right)}{B_{\mathrm{GT}}(\mathrm{g.s.})} = 0.198 \pm 0.024 \quad (68\% \text{ C.L.}). \tag{29}$$

Thus the effects of M_{T} are modest, for the reasons mentioned above. The central value $M_{\mathrm{GT}}(\frac{3}{2}^-) \approx 0.26$ is consistent with the theory range of Table IV, 0.27 ± 0.21.

A similar analysis for the Frekers result for the transition to the 175 keV state yields

$$\begin{matrix} 0.11 \\ 0.065 \end{matrix}\Bigg\} \lesssim \left|M_{\mathrm{GT}}\left(\frac{5}{2}^-\right)\right| \lesssim \begin{cases} 19, & 68\% \text{ C.L.}, \\ 0.23, & 95\% \text{ C.L.}, \end{cases}$$

$$\frac{B_{\mathrm{GT}}\left(\frac{5}{2}^-\right)}{B_{\mathrm{GT}}(\mathrm{g.s.})} = 0.071 \pm 0.036 \quad (68\% \text{ C.L.}). \tag{30}$$

The central value for $|M_{\mathrm{GT}}(\frac{5}{2}^-)| \approx 0.15$ is consistent with the shell-model range, 0.19 ± 0.07.

VI. TOTAL CROSS SECTIONS

The total neutrino cross sections for ^{51}Cr and ^{37}Ar can be expressed in the form [22]

$$\sigma = \sigma_{\text{g.s.}} \left[1 + \xi\left(\frac{5^-}{2}\right) \frac{B_{\text{GT}}\left(\frac{5^-}{2}\right)}{B_{\text{GT}}(\text{g.s.})} + \xi\left(\frac{3^-}{2}\right) \frac{B_{\text{GT}}\left(\frac{3^-}{2}\right)}{B_{\text{GT}}(\text{g.s.})} \right],$$

(31)

where the phase-space coefficients, computed from the results of Table I, are

$$^{51}\text{Cr}: \quad \xi\left(\tfrac{5^-}{2}\right) = 0.669, \quad \xi\left(\tfrac{3^-}{2}\right) = 0.220,$$

$$^{37}\text{Ar}: \quad \xi\left(\tfrac{5^-}{2}\right) = 0.696, \quad \xi\left(\tfrac{3^-}{2}\right) = 0.264. \quad (32)$$

(For earlier calculations of these coefficients see [22,36].)

Combining the excited-state B_{GT} ratios derived from the data of Krofcheck *et al.* [64], Eqs. (26) and (27), with the ground-state result of Eq. (16) yields

$$\sigma(^{51}\text{Cr}) = \begin{cases} 5.69^{+0.28}_{-0.06}, & 68\% \text{ C.L.} \\ 5.69^{+0.51}_{-0.15}, & 95\% \text{ C.L.} \end{cases} \times 10^{-45}\,\text{cm}^2,$$

$$\sigma(^{37}\text{Ar}) = \begin{cases} 6.85^{+0.35}_{-0.08}, & 68\% \text{ C.L.} \\ 6.85^{+0.63}_{-0.20}, & 95\% \text{ C.L.} \end{cases} \times 10^{-45}\,\text{cm}^2. \quad (33)$$

The probability distributions for the cross sections were computed numerically by folding the ground-state and excited-state probabilities. The central values correspond to the most probable cross section and the ranges contain the 68% and 95% fractions of the most probable results. The excited-state contributions increase the cross sections by $\approx 5.6\%$ and 6.2% for ^{51}Cr and ^{37}Ar, respectively.

Repeating this calculation using the excited-state B_{GT} ratios derived from the data of Frekers *et al.* [65], Eqs. (29) and (30), yields

$$\sigma(^{51}\text{Cr}) = \begin{cases} 5.85^{+0.18}_{-0.10}, & 68\% \text{ C.L.} \\ 5.85^{+0.34}_{-0.20}, & 95\% \text{ C.L.} \end{cases} \times 10^{-45}\,\text{cm}^2,$$

$$\sigma(^{37}\text{Ar}) = \begin{cases} 7.02^{+0.19}_{-0.14}, & 68\% \text{ C.L.} \\ 7.02^{+0.38}_{-0.26}, & 95\% \text{ C.L.} \end{cases} \times 10^{-45}\,\text{cm}^2. \quad (34)$$

The excited-state contributions increase the cross sections by $\approx 8.3\%$ and 8.8% for ^{51}Cr and ^{37}Ar sources, respectively. The results of Eqs. (34) and (35) agree at 1σ, but in our view should not be combined because they depend on input strengths for the transition to the $\frac{3^-}{2}$ state that differ by significantly more.

The numerically evaluated cross section distributions can be accurately described as split-normal probability distributions

$$P(\sigma) \approx \sqrt{\frac{2}{\pi}} \frac{1}{\sigma_1 + \sigma_2} [\theta(\bar{\sigma} - \sigma)e^{-(\sigma - \bar{\sigma})^2/2\sigma_1^2}$$

$$+ \theta(\sigma - \bar{\sigma})e^{-(\sigma - \bar{\sigma})^2/2\sigma_2^2}], \quad (35)$$

where σ is dimensionless, in units of $10^{-45}\,\text{cm}^2$. The best fits are obtained by tuning the parameters given above to optimize
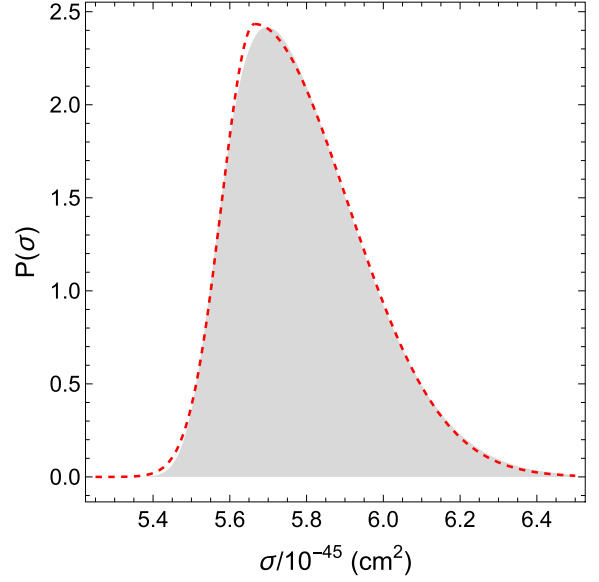

FIG. 3. Shaded region: numerically generated probability distribution for the ^{51}Cr cross section with excited-state contributions extracted from forward-angle (p, n) cross sections of [64] (see text). Dashed line: the analytic split-normal fit to these data.

the overall fit. Figure 3, for the case of a ^{51}Cr source and Krofcheck *et al.* [64] excited state contributions, illustrates the quality of the fit. These split-normal distributions will enable users to adapt our results for any desired confidence level. Table V gives the numerical values for the fit parameters.

Comparisons to past work. In Table VI we compare our cross section result to those obtained by other authors in past years. We briefly comment on the different approaches taken, summarizing a more complete discussion that appears in [78].

(1) Bahcall (1997) [36]. This work included, in its estimate of $\sigma_{\text{g.s.}}$, overlap and exchange atomic effects, and used the then prevailing value of $Q_{\text{EC}} = 232.69 \pm 0.15$ keV. Excited state B_{GT} values were taken from the (p, n) values of [64].

(2) Haxton (1998) [23]. This work pointed out the need to include the tensor interaction when using (p, n) data, and estimated M_{T} from a truncated SM calculation, as spaces of dimension $\approx 10^8$ could not be treated at the time. Because this limited the included correlations, the SM value for M_{T} was taken as an upper bound,

TABLE V. The split normal parametrization of our cross section results.

Source	Excited states	$\bar{\sigma}$	σ_1	σ_2
^{51}Cr	[64]	5.66	0.0854	0.242
^{51}Cr	[65]	5.84	0.115	0.164
^{37}Ar	[64]	6.82	0.108	0.302
^{37}Ar	[65]	6.98	0.135	0.201

TABLE VI. A summary of the published neutrino reaction cross section estimates for $^{71}\text{Ga}(\nu_e, e^-)^{71}\text{Ge}$ in units of 10^{-45} cm^2. All results are given at 68% C.L.

Author	Year	$\sigma(^{51}\text{Cr})$	$\sigma(^{37}\text{Ar})$
Bahcall [36]	1997	$5.81^{+0.21}_{-0.16}$	$7.00^{+0.49}_{-0.21}$
Haxton [23]	1998	6.39 ± 0.68	
Barinov *et al.* [77]	2018	5.91 ± 0.11	7.14 ± 0.15
Kostensalo *et al.* [68]	2019	5.67 ± 0.06	6.80 ± 0.08
Semenov [50]	2020	5.94 ± 0.12	7.17 ± 0.15
Present work	2023	$5.69^{+0.28}_{-0.06}$	$6.85^{+0.35}_{-0.08}$

yielding a large uncertainty on the extracted excited-state contributions.

(3) Barinov *et al.* (2018) [77]. This work used weak couplings updated to 2018 and a value for $Q_{EC} = 233.5 \pm 1.2$ keV obtained from a Penning trap measurement of the mass difference that was later superseded by the more accurate trapping result of [26]. The excited-state GT strengths were extracted from the (p, n) data, without tensor corrections.

(4) Kostensalo *et al.* (2019) [68]. The cross section is taken from SM calculations using the JUN45 interaction, which among the interactions studied here predicts the smallest excited-state GT strengths. From [36] onward investigators have concluded that cross section estimates must be taken from experiment, with theory employed only for corrections (as has been done here): SM wave functions are soft projections (at best) of the true wave function, so lack many of the correlations important in evaluating the interfering amplitudes often responsible for weak transitions.

The JUN45 B_{GT} values for $^{71}\text{Ga}(\nu, e)^{71}\text{Ge}$ to the $\frac{3}{2}^-$ and $\frac{5}{2}^-$ excited states are 2.3×10^{-3} and 5.2×10^{-3}, respectively. We can test the predictive power of JUN45 using transitions of similar but known strengths in closely related nuclei. The B_{GT} values for $^{71}\text{As(EC)}^{71}\text{Ge}$ to the $\frac{3}{2}^-$ and $\frac{5}{2}^-$ states of interest are known: ^{71}As differs from ^{71}Ga only by the conversion of a neutron pair to a proton pair. There are similar testing opportunities using $^{69}\text{Ge(EC)}^{69}\text{Ga}$, which involves parent and daughter nuclei differing from ^{71}Ga and ^{71}Ge only by the removal of a neutron pair. The results are given in Table VII and show large discrepancies between predicted and measured B_{GT} values, in two

cases exceeding an order of magnitude. That is, the table is not encouraging.

(5) Semenov (2020) [50]. This work follows [36] quite closely, treating the excited states as was done there, but utilizing updated weak couplings and and the modern Q_{EC} value of [26].

In previous work, the determinations of σ_{gs} have neglected a series of $\approx 0.5\%$ effects that we have addressed here, including Coulomb corrections computed from realistic nuclear densities consistent with the measured rms charge radius, weak magnetism corrections, and the difference in the radiative correction from bremsstrahlung to the EC and (ν, e) reactions. Here we have addressed such corrections.

Most past work has also taken excited-state contributions directly from forward-angle (p, n) reactions, assuming that a procedure calibrated for strong B_{GT} transitions and gross B_{GT} profiles could be applied to individual weak transitions. However, one expects the typical correction due to M_T to be more important when the dominant amplitude with which it interferes, M_{GT}, is suppressed. This physics, apparent from Fig. 2, has been treated here with as much statistical rigor as possible, propagating input experimental and theoretical errors through to the extracted excited-state cross sections, to quantify their likelihoods. This procedure is limited by the need to quantify the uncertainty on the correction M_T, which must be taken from nuclear models. It is helpful that in the situation of most concern—a weak M_{GT} interfering with a strong M_T, thereby compensating in part for the small value of δ—theory is needed only for the strong matrix element, as the sum is constrained by experiment. The SM has a better track record in such cases. We discussed a common example, an ℓ-forbidden $M1$ transition, where a weak M_{GT} and a strong M_T would arise. Here we have used the variation among SM predictions of M_T to define an uncertainty, with the understanding that there could be additional hidden uncertainties, reflecting common assumptions of the SM affecting all calculations.

VII. IMPACT ON THE BEST AND GALLIUM ANOMALIES

The BEST ^{71}Ge production rates for the outer and inner volumes, obtained from the yields in the K and L peaks with a correction for the contribution of the M peak [20,21], are

$$R_{\text{out}} = 55.6 \pm 2.7\,(\text{stat})^{+1.6}_{-1.5}\,(\text{syst})\,\text{atoms/d}$$
$$= 55.6 \pm 3.1\,\text{atoms/d},$$
$$R_{\text{in}} = 54.9 \pm 2.5\,(\text{stat})^{+1.6}_{-1.5}\,(\text{syst})\,\text{atoms/d}$$
$$= 54.9^{+3.0}_{-2.9}\,\text{atoms/d}, \tag{36}$$

where the statistical and systematic errors have been combined in quadrature to obtain a total error. From the neutrino source activity of 3.414 ± 0.008 MCi and the cross section of Bahcall [36] used in [21], one finds the predicted production rates

$$R_{\text{out}}^{\text{expected}} = 72.6^{+2.6}_{-2.1}\,\text{atoms/d},$$
$$R_{\text{in}}^{\text{expected}} = 69.4^{+2.5}_{-2.0}\,\text{atoms/d}, \tag{37}$$

TABLE VII. Tests of JUN45 against neighboring transitions where $\log(ft)$ values are known from experiment.

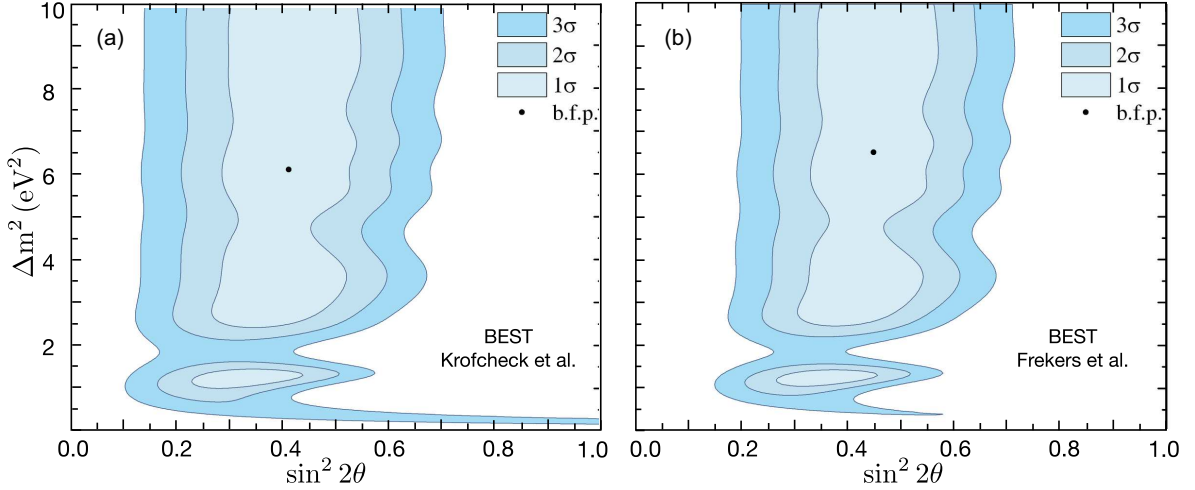| Transition	$\log(ft)$	B_{GT}^{exp}	B_{GT}^{JUN45}
$^{71}\text{As(EC)}^{71}\text{Ge}(\frac{5}{2}^-, 175\,\text{keV})$	5.85	5.3×10^{-3}	6.9×10^{-3}
$^{71}\text{As(EC)}^{71}\text{Ge}(\frac{3}{2}^-, 500\,\text{keV})$	7.19	2.4×10^{-4}	1.8×10^{-5}
$^{69}\text{Ge(EC)}^{69}\text{Ga}(\frac{3}{2}^-, \text{g.s.})$	6.49	1.2×10^{-3}	3.4×10^{-5}
$^{69}\text{Ge(EC)}^{69}\text{Ga}(\frac{5}{2}^-, 574\,\text{keV})$	6.24	2.2×10^{-3}	4.6×10^{-3}

FIG. 4. The allowed regions for oscillations into a sterile state derived from the BEST inner and outer results, which becomes successively wider as the confidence level is increased from 1σ, to 2σ, and then to 3σ. (a) The neutrino absorption cross section derived using the (p, n) data of [64] to constrain excited-state contributions. (b) Results using the $(^3\text{He}, t)$ data of [65]. The best-fit points are $\sin^2 2\theta = 0.41$ and $\Delta m^2 = 6.1 \, \text{eV}^2$ and $\sin^2 2\theta = 0.45$ and $\Delta m^2 = 6.5 \, \text{eV}^2$, respectively (see text).

where again uncertainties have been combined in quadrature. The ratios of the measured to predicted production rates are

$$\frac{R_{\text{out}}}{R_{\text{out}}^{\text{expected}}} = \frac{55.6 \pm 3.1}{72.6_{-2.1}^{+2.6}} \approx 0.77 \pm 0.05,$$

$$\frac{R_{\text{in}}}{R_{\text{in}}^{\text{expected}}} = \frac{54.9_{-2.9}^{+3.0}}{69.4_{-2.0}^{+2.5}} \approx 0.79 \pm 0.05, \qquad (38)$$

showing discrepancies of 4.7 and 4.2 standard deviations, respectively. The ratio of the outer and inner rate ratios,

$$r = \frac{R_{\text{out}}/R_{\text{out}}^{\text{expected}}}{R_{\text{in}}/R_{\text{in}}^{\text{expected}}} = \frac{0.77 \pm 0.05}{0.79 \pm 0.05} \approx 0.97 \pm 0.09, \quad (39)$$

is consistent with unity, revealing no dependence on distance from the source.

The Bahcall cross section used above employed the (p, n) data of Krofcheck et al. [64] in estimating the excited-state contribution to the ^{71}Ga cross section. The analogous analysis presented here, updating the ground-state contribution and correcting for the tensor contribution to the (p, n) results of [64], yields

$$R_{\text{out}}^{\text{expected}} = 71.1_{-0.8}^{+3.5} \text{ atoms/d},$$

$$R_{\text{in}}^{\text{expected}} = 68.0_{-0.7}^{+3.3} \text{ atoms/d}. \qquad (40)$$

The ratios of the measured to predicted production rates are

$$\frac{R_{\text{out}}}{R_{\text{out}}^{\text{expected}}} = \frac{55.6 \pm 3.1}{71.1_{-0.8}^{+3.5}} \approx 0.78 \pm 0.05,$$

$$\frac{R_{\text{in}}}{R_{\text{in}}^{\text{expected}}} = \frac{54.9_{-2.9}^{+3.0}}{68.0_{-0.7}^{+3.3}} \approx 0.81 \pm 0.05. \qquad (41)$$

As the cross section derived here is slightly reduced from that [36] used in the original BEST analysis [20,21], the deviation of R from 1 is also slightly reduced.

We have also constrained the ^{71}Ge excited-state contribution using the $(^3\text{He}, t)$ data of Frekers et al. [65]. This yields

$$R_{\text{out}}^{\text{expected}} = 73.1_{-1.3}^{+2.3} \text{ atoms/d},$$

$$R_{\text{in}}^{\text{expected}} = 69.9_{-1.2}^{+2.2} \text{ atoms/d}. \qquad (42)$$

The ratios of the measured to predicted production rates are

$$\frac{R_{\text{out}}}{R_{\text{out}}^{\text{expected}}} = \frac{55.6 \pm 3.1}{73.1_{-1.3}^{+2.3}} \approx 0.76 \pm 0.05,$$

$$\frac{R_{\text{in}}}{R_{\text{in}}^{\text{expected}}} = \frac{54.9_{-2.9}^{+3.0}}{69.9_{-1.2}^{+2.2}} \approx 0.79 \pm 0.05, \qquad (43)$$

reflecting the somewhat stronger transition to the $\frac{3}{2}^-$ extracted from the $(^3\text{He}, t)$ data.

The combined result from all six Ga calibration experiments [21] for the ratio of the measured to expected rates is 0.82 ± 0.03, using the cross section derived here, taking the excited-state data from [64], and treating all measurements as independent. However, as discussed in [78], when possible correlations among the measurements are taken into account, this is revised to 0.82 ± 0.05.

Although the cross section changes found here are modest, we have updated the neutrino oscillation results of [20,21]. Figure 4 gives the exclusion contours corresponding to 1σ, 2σ, and 3σ confidence levels, using only the BEST inner and outer results. The cross sections used are those derived here, with the excited-state contribution extracted from the results of [64] (left panel) and [65] (right panel). The best-fit points correspond to $\sin^2 2\theta = 0.41$ and $\Delta m^2 = 6.1 \, \text{eV}^2$ and $\sin^2 2\theta = 0.45$ and $\Delta m^2 = 6.5 \, \text{eV}^2$, respectively. However, the chi-square space is quite shallow and flat, so solutions along a valley centered on the contours of Figs. 4 and 5 provide nearly equivalent fits.

Figure 5 gives the exclusion contours corresponding to 1σ, 2σ, and 3σ confidence levels, when the BEST inner and
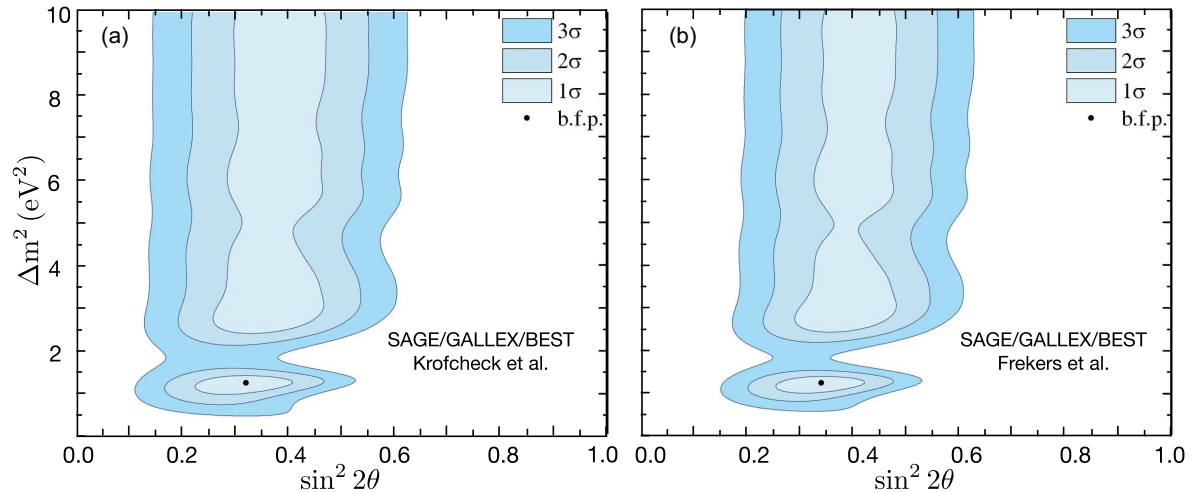
FIG. 5. As in Fig. 4, but combining the results of the two GALLEX and two SAGE calibrations with those of BEST. The best-fit points are $\sin^2 2\theta = 0.32$ and $\Delta m^2 = 1.25\,\text{eV}^2$ (left) and $\sin^2 2\theta = 0.34$ and $\Delta m^2 = 1.25\,\text{eV}^2$ (right).

outer results are combined with those of the two GALLEX and two SAGE calibrations. The best-fit points correspond to $\sin^2 2\theta = 0.32$ and $\Delta m^2 = 1.25\,\text{eV}^2$ and $\sin^2 2\theta = 0.34$ and $\Delta m^2 = 1.25\,\text{eV}^2$, respectively, for the indicated cross sections. The shift in the best-fit results from those of Fig. 4 reflect the shallowness of the chi-square space.

VIII. SUMMARY AND CONCLUSIONS

The published BEST analysis employed an older ^{51}Cr cross section from Bahcall [36], $\sigma = [5.81^{+0.21}_{-0.16}] \times 10^{-45}\,\text{cm}^2$ (1σ). Due to the experiment's surprising result, there is good motivation for reexamining the neutrino capture cross section on ^{71}Ga, to determine both a more modern best value for the cross section and its uncertainty. The latter is particularly important in judging the significance of the BEST result. The cross section is dominated by the transition to the ground state of ^{71}Ge. Since the work of [36], changes impacting this cross section include a more accurate Q value and updates in the value of g_A and other weak parameters. In addition, there are effects such as weak magnetism and the lack of universality in radiative corrections that have not previously been evaluated quantitatively. The first half of this paper describes these and other corrections that typically each enter at the 0.5% level. We have evaluated these effects including their uncertainties, finding that they combine to yield a ground-state cross section about 2.4% smaller than that of Bahcall [36].

However, the more serious potential uncertainty is that associated with the transitions to the 175 keV $\frac{5}{2}^-$ and 500 keV $\frac{3}{2}^-$ excited states in ^{71}Ge. In [36] those cross sections were taken from forward-angle (p, n) measurements by Krofcheck *et al.* [64]. As was stressed in [22,23] and illustrated here in Fig. 2, (p, n) scattering is not a reliable probe of weak B_{GT} strengths due to the presence of a subdominant spin-tensor interaction in the effective operator for the scattering. While normally a correction, the tensor operator can dominate when the competing GT amplitude is weak. Haxton and Hata

stressed that ^{71}Ga is a problematic case, as the transition to the first excited state, $\frac{3}{2}^- \rightarrow \frac{5}{2}^-$ (175 keV), is naturally associated with the ℓ-forbidden amplitude $2p_{3/2} \rightarrow 1f_{5/2}$. This observation was confirmed here in all three of the shell-model calculations performed. For a pure ℓ-forbidden transition, the GT amplitude is zero, while the tensor amplitude would have approximately unit strength [22].

The relationship between GT strength and (p, n) forward scattering would be restored if one could quantitatively correct for the presence of the tensor operator. This would be possible if one could (1) reliably determine the coefficient δ of the tensor correction (its size and uncertainty) and (2) develop some means of determining the accuracy with which the accompanying nuclear matrix element of the tensor operator can be determined. Despite previous work [22,23,66] determining δ from experiment, the simple fits performed and the rather uncritical selection of data left questions about the certainty with which δ could be established.

In this paper we determine δ using only measurements where experimental uncertainties have been assigned and focusing on transitions involving relatively simple $1p$- and $2s1d$-shell nuclei where structure differences arising from the choice of shell-model effective interaction are small. Where possible, nuclear structure differences were quantified by exploring several effective interactions. An attractive aspect of this approach is that an accurate evaluation of the tensor matrix element is most important in those cases where it is strong, and these are cases where the shell model should do well. We see from Table II that, in the four $2s1d$-shell cases where the tensor matrix element is ≈ 1, the variation among the calculations is typically 10%. Consequently, in transitions where the GT amplitude is weak but the tensor amplitude strong, one can use theory to estimate the latter (but not the former) reliably, and thus subtract it; the 10% error enters in the correction, not in end result. With a more quantitative relationship between (p, n) measurements and GT amplitudes thus restored, even relatively weak M_{GT} can then be extracted from the data.

In determining δ, we found a very strong correlation between cases where (p, n) and weak transition strengths disagreed, and strong tensor matrix elements producing a ratio of $|M_{\mathrm{T}}/M_{\mathrm{GT}}|$ well above 1. Our study also underscores the fact that the weakness of excited-state contributions to the ^{71}Ga cross section place them in a category of transitions where important tensor corrections arise. After folding in uncertainties from both experiment and theory, we found that $\delta = 0.074 \pm 0.008\,(1\sigma)$. As shown in Fig. 2, when the tensor correction is made with this value of δ, excellent agreement between (p, n) cross sections and weak transition strengths is restored, even for weak GT transitions. To the precision that δ can be determined from the available data, there is no statistical evidence for any variation with mass number: our global fit and fits to individual transitions spanned a factor of 3 in mass number, from ^{13}C to ^{39}K.

As this value of δ works well for a range of $2s1d$- and $1p$-shell nuclei, the use of the same δ in the $2p1f$ shell is reasonable. This leaves the second issue mentioned above, the need to evaluate uncertainties associated with theory estimates of the accompanying matrix element M_{T}. While the nuclear structure of ^{71}Ga is more complex than that of the $1p$- and $2s1d$-shell nuclei used in our extraction of δ, the three large-basis, full-space $2p_{3/2}1f_{5/2}2p_{1/2}1g_{9/2}$ shell-model calculations we performed were reasonably consistent in their predictions of the magnitude of M_{T} and sign relative to M_{GT}. Though the spread in M_{T} is larger than found in our $1p$- and $2s1d$-shell calculations, this spread was incorporated into a theory uncertainty that was then propagated through our analysis. With the correction for M_{T} made, we then extracted the needed excited state GT strengths from the (p, n) and $(^3\mathrm{He}, t)$ results of [64] and [65], respectively.

The analysis shows that M_{T} and M_{GT} interfere destructively in both excited-state transitions, which increases the $|M_{\mathrm{GT}}|$ extracted from experiment. Consequently, the excited-state contribution to the total ^{51}Cr cross section is increased modestly, to $\approx 6\%$ and $\approx 8\%$, depending on whether the data from [64] or [65] is used. The result we obtained from the data of [64], $[5.69^{+0.28}_{-0.06}] \times 10^{-45}\,\mathrm{cm}^2\,(1\sigma)$ can be compared to the analogous result of Bahcall employed in the BEST analysis, $[5.81^{+0.21}_{-0.16}] \times 10^{-45}\,\mathrm{cm}^2\,(1\sigma)$. The results are in agreement at 1σ, reflecting in part compensating changes in the present analysis due to a weaker ground-state and stronger excited-state contributions.

Several objections that one might have raised to the use of an older cross section — including a more naïve use of the (p, n) data, absence of radiative and weak-magnetism corrections, and various changes in weak parameters and Coulomb corrections — have been addressed and in combination have been found to shift the recommended central value by only 2%. Most important, the analysis presented here has propagated all identified errors — whether experimental or theoretical — through to the end result. Thus the error bars reflect all known uncertainties, to the precision currently possible. Finally, taking into account uncertainties, the extracted values of M_{GT} are in agreement with the predictions of the shell model. While we would certainly not advocate use of theory in estimating such weak B_{GT} strengths, nevertheless this consistency is of some comfort, as the shell model is employed in the evaluation of the correction terms proportional to M_{T}.

Finally, we note that a 3% larger cross section is obtained if we base the excited-state analysis on the $(^3\mathrm{He}, t)$ data of [65]. There would be some value in repeating both the (p,n) and $(^3\mathrm{He}, t)$ measurements: while the impact on the cross section is modest, the difference in the cross sections for exciting the $\frac{3}{2}^-$ state exceeds expectations, given the assigned error bars.

The lower cross section derived here from the (p, n) data of [64] slightly reduces the size of the BEST and Ga anomalies (by $\approx 2\%$), but certainly does not remove them. We have demonstrated this by repeating the sterile-neutrino oscillation analysis of [20,21], finding small shifts in the confidence-level contours and best-fit values for $\sin^2 2\theta$ and Δm^2. The very well measured ground-state transition σ_{gs} establishes a floor on the cross section just 8% below the value used in the BEST and earlier Ga analyses. Even if this minimum theoretical floor were to be used — the revised value found here is $[5.39 \pm 0.04] \times 10^{-45}\,\mathrm{cm}^2\,(1\sigma)$ — the existing discrepancies would be reduced by about half, but not eliminated. Furthermore, we stress that use of such an extreme minimum cross section would not be consistent with the present analysis, as that value lies well beyond the 95% C.L. lower bound on the total cross section derived here.

[1] M. A. Acero, C. A. Argüelles, N. Hostert, D. Kaira, G. Karagiorgi *et al.*, arXiv:2203.07323.

[2] K. N. Abazajian, M. A. Acero, S. K. Agarwalla, A. A. A.-Arevalo, C. H. Albright *et al.*, arXiv:1204.5379.

[3] S. Gariazzo, C. Giunti, M. Laveder, Y. F. Li, and E. M. Zavanin, J. Phys. G: Nucl. Part. Phys. **43**, 033001 (2016).

[4] C. Giunti and T. Lasserre, Annu. Rev. Nucl. Part. Sci. **69**, 163 (2019).

[5] S. Böser, C. Buck, C. Giunti, J. Lesgourgues, L. Ludhova, S. Mertens, A. Schukraft, and M. Wurm, Prog. Part. Nucl. Phys. **111**, 103736 (2020).

[6] A. Diaz, C. Arguelles, G. Collin, J. Conrad, and M. Schaevitz, Phys. Rep. **884**, 1 (2020).

[7] S.-H. Seo, in *19th Lomonosov Conference on Elementary Particle Physics* (Moscow State Univ., 2019).

[8] B. Dasgupta and J. Kopp, Phys. Rep. **928**, 1 (2021).

[9] A. de Gouvêa, G. J. Sánchez, and K. J. Kelly, Phys. Rev. D **106**, 055025 (2022).

[10] K. Abe *et al.* (Super-Kamiokande Collaboration), Phys. Rev. D **94**, 052010 (2016).

[11] B. Aharmim *et al.* (SNO Collaboration), Phys. Rev. C **88**, 025501 (2013).

[12] M. Agostini *et al.* (Borexino Collaboration), Astrophys. J. **850**, 21 (2017).

[13] S. Appel *et al.*, Phys. Rev. Lett. **129**, 252701 (2022).

[14] W. C. Haxton, R. G. H. Robertson, and A. M. Serenelli, Annu. Rev. Astron. Astrophys. **51**, 21 (2013).

[15] G. D. Orebi Gann, K. Zuber, D. Bemmerer, and A. Serenelli, Annu. Rev. Nucl. Part. Sci. **71**, 491 (2021).

[16] P. Anselmann, R. Frockenbrock, W. Hampel, G. Heusser, J. Kiko *et al.* (GALLEX Collaboration), Phys. Lett. B **342**, 440 (1995).

[17] J. N. Abdurashitov, V. N. Gavrin, S. V. Girin, V. V. Gorbachev, T. V. Ibragimova, A. V. Kalikhov *et al.*, Phys. Rev. C **59**, 2246 (1999).

[18] W. Hampel, G. Heusser, J. Kiko, T. Kirsten, M. Laubenstein *et al.*, Phys. Lett. B **420**, 114 (1998).

[19] J. N. Abdurashitov, V. N. Gavrin, S. V. Girin, V. V. Gorbachev, P. P. Gurkina, T. V. Ibragimova *et al.*, Phys. Rev. C **73**, 045805 (2006).

[20] V. V. Barinov, B. T. Cleveland, S. N. Danshin, H. Ejiri, S. R. Elliott, D. Frekers, Phys. Rev. Lett. **128**, 232501 (2022).

[21] V. V. Barinov, S. N. Danshin, V. N. Gavrin, V. V. Gorbachev, D. S. Gorbunov, T. V. Ibragimova *et al.*, Phys. Rev. C **105**, 065502 (2022).

[22] N. Hata and W. C. Haxton, Phys. Lett. B **353**, 422 (1995).

[23] W. C. Haxton, Phys. Lett. B **431**, 110 (1998).

[24] W. Hampel and L. P. Remsberg, Phys. Rev. C **31**, 666 (1985).

[25] B. Sigh and J. Chen, Nucl. Data Sheets **188**, 1 (2023).

[26] M. Allansary, D. Frekers, T. Eronen, L. Canete, J. Hakala *et al.*, Int. J. Mass Spectrom. **406**, 1 (2016).

[27] J. N. Abdurashitov, V. N. Gavrin, S. V. Girin, V. V. Gorbachev, T. V. Ibragimova, A. V. Kalikhov *et al.*, Phys. Rev. C **60**, 055801 (1999).

[28] P. Benois-Gueutal, Comp. Rend. **230**, 624 (1950).

[29] S. Odiot and R. Daudel, J. Phys. Radium **17**, 60 (1956).

[30] J. N. Bahcall, Phys. Rev. Lett. **9**, 500 (1962).

[31] E. Vatai, Nucl. Phys. A **156**, 541 (1970).

[32] J. N. Bahcall, Phys. Rev. **131**, 1756 (1963).

[33] J. N. Bahcall, Phys. Rev. **132**, 362 (1963).

[34] J. N. Bahcall, Nucl. Phys. **71**, 267 (1965).

[35] B. Märkisch, H. Mest, H. Saul, X. Wang, H. Abele, Phys. Rev. Lett. **122**, 242501 (2019).

[36] J. N. Bahcall, Phys. Rev. C **56**, 3391 (1997).

[37] A. Gniady, E. Caurier, and F. Nowacki (unpublished).

[38] B. A. Brown (unpublished); B. Cheal, E. Mané, J. Billowes, M. L. Bissell, K. Blaum, B. A. Brown *et al.*, Phys. Rev. Lett. **104**, 252502 (2010).

[39] M. Honma, T. Otsuka, T. Mizusaki, and M. Hjorth-Jensen, Phys. Rev. C **80**, 064323 (2009).

[40] J. G. Hirsch and P. C. Srivastava, J. Phys.: Conf. Ser. **387**, 012020 (2012).

[41] E. Mane, B. Cheal, J. Billowes, M. L. Bissell, K. Blaum, F. C. Charlwood *et al.*, Phys. Rev. C **84**, 024303 (2011).

[42] P. C. Srivastava, J. Phys. G: Nucl. Part. Phys. **39**, 015102 (2012).

[43] P. Klos, J. Menendez, D. Gazit, and A. Schwenk, Phys. Rev. D **88**, 083516 (2013).

[44] E. Caurier, J. Menendez, F. Nowacki, and A. Poves, Phys. Rev. Lett. **100**, 052503 (2008).

[45] J. Menendez, A. Poves, E. Caurier, and F. Nowacki, Phys. Rev. C **80**, 048501 (2009).

[46] C. W. Johnson, W. E. Ormand, and P. G. Krastev, Comput. Phys. Commun. **184**, 2761 (2013).

[47] C. W. Johnson, W. E. Ormand, K. S. McElvain, and H. Shan, arXiv:1801.08432.

[48] A. Sirlin, Rev. Mod. Phys. **50**, 573 (1978).

[49] A. Kurylov, M. J. Ramsey-Musolf, and P. Vogel, Phys. Rev. C **67**, 035502 (2003).

[50] S. V. Semenov, Phys. At. Nuclei **83**, 1549 (2020).

[51] D. H. Wilkinson, Nucl. Instrum. Methods Phys. Res., Sect. A **335**, 182 (1993).

[52] L. Hayen, N. Severijns, K. Bodek, D. Rozpedzik, and X. Mougeot, Rev. Mod. Phys. **90**, 015008 (2018).

[53] H. Behrens and H. Jänecke, in *Numerical Tables for Beta Decay and Electron Capture*, edited by K.-H. Hellwege (Springer-Verlag, Berlin, 1969).

[54] H. De Vries, C. W. De Jaeger, and C. De Vries, At. Data Nucl. Data Tables **36**, 495 (1987).

[55] D. H. Wilkinson, Nucl. Instrum. Methods Phys. Res., Sect. A **290**, 509 (1990).

[56] M. E. Rose, Phys. Rev. **49**, 727 (1936).

[57] A. Czarnecki, G. P. Lepage, and W. J. Marciano, Phys. Rev. D **61**, 073001 (2000).

[58] V. A. Kuzmin, Sov Phys. JETP **22**, 1051 (1966) [Zh. Eksp. Teor. Fiz. **49**, 1532 (1965)].

[59] J. N. Bahcall, Rev. Mod. Phys. **50**, 881 (1978).

[60] A. J. Baltz, J. Weneser, B. A. Brown, and J. Rapaport, Phys. Rev. Lett. **53**, 2078 (1984).

[61] G. J. Mathews, S. D. Bloom, G. M. Fuller, and J. N. Bahcall, Phys. Rev. C **32**, 796 (1985).

[62] K. Ikeda, Prog. Theor. Phys. **31**, 434 (1964); J. I. Fujita and K. Ikeda, Nucl. Phys. **67**, 145 (1965).

[63] See, e.g., T. N. Taddeucci *et al.*, Nucl. Phys. A **469**, 125 (1987).

[64] D. Krofcheck *et al.*, Phys. Rev. Lett. **55**, 1051 (1985); Ph.D. thesis, Ohio State University, 1987 (unpublished), see Table D-7.

[65] D. Frekers *et al.*, Phys. Lett. B **706**, 134 (2011).

[66] J. W. Watson *et al.*, Phys. Rev. Lett. **55**, 1369 (1985).

[67] P. vonNeumann-Cosel and J. N. Ginocchio, Phys. Rev. C **62**, 014308 (2000).

[68] J. Kostensalo, J. Suhonen, C. Giunti, and P. C. Srivastava, Phys. Lett. B **795**, 542 (2019). We believe there is a numerical error in this work affecting the computation of M_{T}.

[69] B. D. Anderson *et al.*, Phys. Rev. C **27**, 1387 (1983).

[70] R. G. T. Zegers, H. Akimune, S. M. Austin, D. Bazin, A. M. vandenBerg, G. P. A. Berg *et al.*, Phys. Rev. C **74**, 024309 (2006).

[71] E. W. Grewe, C. Baumer, A. M. van den Berg, N. Blasi, B. Davids, D. De Frenne *et al.*, Phys. Rev. C **69**, 064325 (2004).

[72] See https://www.nndc.bnl.gov.

[73] S. Cohen and D. Kurath, Nucl. Phys. **73**, 1 (1965).

[74] B. A. Brown and H. Wildenthal, Annu. Rev. Nucl. Part. Sci. **38**, 29 (1988).

[75] B. A. Brown and W. A. Richter, Phys. Rev. C **74**, 034315 (2006).

[76] D. Frekers, P. Puppe, J. H. Thies, and H. Ejiri, Nucl. Phys. A **916**, 219 (2013).

[77] V. Barinov, B. Cleveland, V. Gavrin, D. Gorbunov, and T. Ibragimova, Phys. Rev. D **97**, 073001 (2018).

[78] S. R. Elliott, V. Gavrin, and W. C. Haxton, arXiv:2306.03299.